NASA CR-82456
FOLH.
1967
v. 2
Ex. 1
INPE - Bibl.
LCP
58.608
942749

ROCKET RESEARCH CORPORATION

DEVELOPMENT OF DESIGN AND SCALING CRITERIA FOR MONOPROPELLANT HYDRAZINE REACTORS EMPLOYING

A Reproduced Copy

OF

N67-19123

Reproduced for NASA

by the

NASA Scientific and Technical Information Facility

FFNo 672 Aug 65

PRECEDING PAGE BLANK NOT FILMED.

2.0 HYDRAZINE MONOPROPELLANT PROPERTIES

Hydrazine is a thermochemically unstable liquid which under certain conditions undergoes exothermic decomposition with the release of heat. The physical properties of hydrazine are similar to those of water. General properties of hydrazine are listed in Table I.

Two reactions are involved in the decomposition of hydrazine:

$$N_2H_4 \longrightarrow \frac{4}{3} NH_3 + \frac{1}{3} N_2 + 144{,}300 \text{ Btu} \qquad (1)$$

$$NH_3 \longrightarrow \frac{3}{2} H_2 + \frac{1}{2} N_2 - 79{,}200 \text{ Btu} \qquad (2)$$

The second reaction is usually incomplete and can be controlled to some extent by limiting catalyst bed length. The overall reaction is commonly expressed as (Reference 3):

$$3N_2H_4 \longrightarrow 4(1 - X) NH_3 + (2X + 1) N_2 + 6X H_2 + (144{,}300 - 79{,}200X) \text{ Btu} \qquad (3)$$

where X is the percent of ammonia dissociation. Figure 1 shows specific impulse for 1000/14.7 psia, characteristic velocity, gas molecular weight, and gas temperature as a function of ammonia dissociation. Additional performance data on monopropellant hydrazine and mixtures of hydrazine, hydrazinium nitrate, and water is presented in Reference 6.

Ma Ipris
NASA
Em: 29 JUL 1986

ROCKET RESEARCH CORPORATION

FACILITY FORM 602
N67 19123 (ACCESSION NUMBER)
99 (PAGES)
CR-82456 (NASA CR OR TMX OR AD NUMBER)
1 (THRU)
(CODE)
28 (CATEGORY)

Seattle, Washington

mail dic. 15.8.86
CD

DEVELOPMENT OF DESIGN AND SCALING CRITERIA FOR MONOPROPELLANT HYDRAZINE REACTORS EMPLOYING SHELL 405 SPONTANEOUS CATALYST

RRC-66-R-76 - Volume II

Final Report

Prepared under NASA Contract NAS 7-372

Submitted To:

NASA Western Operations Office

Santa Monica, California

By

Rocket Research Corporation

Seattle, Washington

Approved by:

B. W. Schmitz, Project Manager

W. W. Smith, Manager
Hydrazine Programs

January 18, 1967

TABLE OF CONTENTS

		Page
	SUMMARY	
1.0	INTRODUCTION	1
2.0	HYDRAZINE MONOPROPELLANT PROPERTIES	3
3.0	CATALYST BED PROPERTIES	5
4.0	INJECTOR DESIGN CRITERIA	7
5.0	AMMONIA DISSOCIATION	13
6.0	CATALYST BED LENGTH REQUIREMENTS	21
7.0	CATALYST BED PRESSURE DROP	25
8.0	CHAMBER PRESSURE RESPONSE TIME	29
9.0	APPLICATION OF EQUATIONS TO REACTOR DESIGN	41
	9.1 Rocket Engine Design	41
	9.2 Gas Generator Design	43
	APPENDIX I	75
	APPENDIX II	83
	NOMENCLATURE	87
	REFERENCES	91

LIST OF FIGURES

Figure Number		Page
1	Hydrazine Performance Curves (100% N_2H_4)	45
2	Catalyst Bed Porosity vs Catalyst Bed Diameter for 1/8" x 1/8" Cylinders	46
3	Catalyst Bed Porosity Vs. Catalyst Bed Diameter for 1/8" x 1/16" Cylinders	47
4	Catalyst Bed Porosity Vs. Catalyst Bed Diameter for 5-8 Mesh Granular Particles	48
5	Catalyst Bed Porosity Vs. Catalyst Bed Diameter for 10-20 Mesh Granular Particles	49
6	Catalyst Bed Porosity Vs. Catalyst Bed Diameter for 20-30 Mesh Granular Particles	50
7	Effect of Bed Loading on Ammonia Dissociation for 50 lbf Engine	51
8	Effect of Bed Loading on Ammonia Dissociation for 5 lbf Engine, Chamber Pressure = 225 psia	52
9	Effect of Bed Loading on Ammonia Dissociation for 0.5 lbf Engine, Chamber Pressure = 225 psia	53
10	Ammonia Dissociation Model Schematic	54
11	Ratio of Residence Time to Chamber Pressure Vs. Bed Loading for 5 lbf Engine	55
12	Ratio of Residence Time to Chamber Pressure Vs. Bed Loading for 50 lbf Engine	56
13	Ratio of Residence Time to Chamber Pressure Vs. Bed Loading for 0.5 lbf Engine	57
14	Effect of Bed Loading, Residence Time, and Chamber Pressure Fractional Ammonia Dissociation for 5 lbf Engine	58
15	Effect of Bed Loading, Residence Time, and Chamber Pressure on Fractional Ammonia Dissociation for 50 lbf Engine	59
16	Correlation of Ammonia Dissociation Data, 0.5 lbf Engine	60
17	General Correlation of Ammonia Dissociation Data	61
18	Effect of Chamber Pressure on Catalyst Bed Length Requirements, 5 lbf Engine	62
19	Effect of Chamber Pressure on Catalyst Bed Length Requirements, 50 lbf Engine	63
20	Effect of Bed Loading on Catalyst Bed Length Requirements, 5 lbf Engine	64

LIST OF FIGURES (Cont'd)

Figure Number		Page
21	Effect of Bed Loading on Catalyst Bed Length Requirements, 50 lbf Engine	65
22	Correlation of Catalyst Bed Length Requirements	66
23	Correlation of Catalyst Bed, Pressure Drop Data with Grant's Equation	67
24	5 lbf Engine Catalyst Bed Pressure Drop Modified Ergun Equation Correlation	68
25	Pressure Rise Model Schematic, Stage 1	69
26	Pressure Rise Model Schematic, Stage 2	70
27	Stage 1 Pressure Rise Integral Evaluation	71
28	Evaluation of Stage 1 Pressure Rise Constant	72
29	Stage 2 Pressure Rise Integral Evaluation	73
30	Evaluation of Stage 2 Pressure Rise Constant	74

LIST OF TABLES

Table Number		
I	Hydrazine Properties	4

SUMMARY

Under NASA Contract NAS 7-372, issued by NASA Western Operations Office and technically managed by the Jet Propulsion Laboratory, Rocket Research Corporation, Seattle, Washington, undertook a program for the development of design and scaling formulae for monopropellant hydrazine reactors employing the Shell 405 spontaneous catalyst. The enclosed document represents Volume II of the final report on the contract. Volume I presents the contract scope, test plan, engine designs employed, and summarizes the test data obtained.

The enclosed document, Volume II, presents the correlation of the test data into design and scaling formulae and represents a design manual for monopropellant hydrazine reactors employing the Shell 405 spontaneous catalyst. Design formulae are presented to define catalyst bed configuration, ammonia dissociation, catalyst bed pressure drop, and chamber pressure response time as a function of reactor design parameters. Design parameters studied included chamber pressure from 50 to 1,000 psia, bed loading from 0.01 to 0.045 lbm/in^2-sec, catalyst bed length from that required for satisfactory (smooth) operation to a value which resulted in approximately 85% ammonia dissociation, and catalyst particle sizes from 1/8" x 1/8" cylindrical pellets to 25-30 mesh size granules.

An empirical equation was developed which defines the required catalyst bed configuration for smooth, stable, steady-state operation as a function of chamber pressure, bed loading and catalyst particle size. This equation was demonstrated over a thrust range of 0.5 to 100 lbf.

Ammonia dissociation which takes place in the reactor was found to be strongly affected by diffusion of the ammonia to the catalyst surface. A theoretical model assuming diffusion controlled ammonia dissociation resulted in correlation parameters which adequately fit the test data. Because of the high activity of the catalyst it was found that ammonia dissociations below 50% could not be realized and still obtain satisfactory reactor operation.

Catalyst bed pressure drop was found to be adequately predicted by equations developed by Grant (Reference 3) in his work with nonspontaneous catalyst. The Ergun equation correlated well with test data at Reynolds Numbers less than 2000.

The chamber pressure response time was treated as a two stage process in which gas accumulation in the reactor was the initial predominant factor in response time with catalyst heating being predominant in the second stage. A theoretical model was developed and modified empirically to account for kinetic and vaporization effects. This semi-empirical model correlated well with all test data obtained on the program.

TABLE I

HYDRAZINE PROPERTIES

Vapor Pressure @ 68°F	0.205 psia
Density @ 68°F	1.01 gm/cc
Freezing Point	34°F
Viscosity @ 70°F	1.0×10^{-5} ft^2/sec
Shock Sensitivity	0 cards
Impact Sensitivity	> 120 Kg-cm
Thermal Stability (temperature @ onset of rapid decomposition)	ca 400°F
Flash Point	ca 126°F
Toxicity (threshold limit)	1 ppm

1.0 INTRODUCTION

This document constitutes Volume II of the final report of Rocket Research Corporation "Development of Design and Scaling Criteria for Monopropellant Hydrazine Reactors Employing Shell 405 Spontaneous Catalyst" program conducted under contract to NASA Western Operations Office, Santa Monica, California, Contract NAS 7-372. This volume covers the development of theoretical models of reactor operation and presents the correlation analysis conducted to develop the design and scaling criteria. This volume represents a design manual for monopropellant hydrazine rocket engines and gas generators employing the Shell 405 spontaneous catalyst.

Reverse Side Blank

3.0 CATALYST BED PROPERTIES

Catalyst bed porosity measurements were made for cylindrical pellets and varying mesh size graunules of catalyst for varying bed diameters. Cylindrical pellets 1/8" x 1/8" and 1/8" x 1/16" and graunules ranging from 5 to 30 mesh size were packed in cylinders approximately 3.3 inches long of varying diameters of 0.5, 1.0, 1.7, 2.3, 3.0, and 4.0 inches to obtain the required data. In all cases the catalyst was packed within the container in a random dense manner (see Section 7.0). Measurement of the weight of catalyst packed in a container of given volume allows determination of the catalyst bed density. These measurements are then converted to catalyst bed porosity by use of the catalyst particle density using the following equation:

$$\epsilon = 1 - \frac{\rho_b}{\rho_p} \tag{4}$$

Where:

ϵ = Catalyst bed porosity

ρ_b = Catalyst bed density

ρ_p = Catalyst particle density

Data on catalyst and/or carrier particle density was supplied by Shell Development Company. The catalyst particle density was measured by a mercury porosimeter in which particle pores and spaces down to 20 microns are excluded from the particle.

The measurements of catalyst bed porosity are summarized in Figures 2 through 6, wherein catalyst bed porosity is plotted as a function of catalyst bed diameter for the various catalyst sizes and shapes. The 6-8 mesh catalyst has an average particle size of 0.121 inches which is very close to the 1/8 x 1/8 inch pellets. It is interesting to note that for the same size particle, the cylindrical pellets have a lower catalyst bed porosity than do the granular pellets.

Catalyst bed specific surface area was calculated from the bed porosity measurements through the use of the following equation (Reference 7):

$$A_s = \frac{6(1 - \epsilon)}{\phi_s d_p} \tag{5}$$

Where:

A_s = Catalyst bed specific surface area

ϵ = Catalyst bed porosity

ϕ_s = Sphericity of the particle

d_p = Particle size

The sphericity of the 1/8 x 1/8 inch and 1/8 x 1/16 inch cylindrical pellets was calculated to be 0.874 and 0.825 respectively. An average sphericity of 0.75 (Reference 7) was assumed for all sizes of granular particles. The catalyst specific surface area is depicted in Figures 2 through 6 as a function of catalyst bed diameter for the particles sizes and shapes investigated.

The catalyst particle density was measured as 0.079 lbm/in^3. Thus, the weight of catalyst in a given volume chamber may be calculated using Equation 4 as:

$$W_c = (0.079)(1 - \epsilon)(V_c)$$

Certain calculations make use of an equivalent spherical particle diameter defined such that the volume of the sphere has the same volume as the volume of the particle in question. The equivalent spherical diameter of a particle may be estimated from (Reference 6):

$$d_s = \left(\frac{6}{\pi} K_v\right)^{1/3} d_p$$

Where:

d_s = Diameter of a spherical particle which has the same volume as the volume of the particle in question, in

d_p = Average particle diameter, in

K_v = Volumetric shape factor

For granular particles K_v is approximately 0.27 and for cylinders with an L/D of 1.0, K_v is equal to 0.785.

4.0 INJECTOR DESIGN CRITERIA

The purpose of the injector test program was to conduct a performance comparison of two distinct injector configurations at the .5 lbf, 5 lbf, and 50 lbf thrust levels while varying injector hydraulic pressure drop, propellant mass distribution across the face of the injector, and the distance between the injector and the top of the catalyst bed. The designs chosen for the study were a drilled orifice showerhead design and a modified showerhead design employing porous sintered woven wire sheet elements (trade name "Rigimesh") in lieu of drilled orifices. The superior performing injector was then selected for subsequent bed loading, chamber pressure, and catalyst bed length studies. This phase of the study was not aimed at determining and characterizing the optimum injector for monopropellant hydrazine catalyst reactors. Rather, it was aimed at selecting a stable and well performing injector design which would not introduce unwanted injector performance variations during conduct of the catalyst bed scaling law tests. It is recognized that several alternate injector designs to those described here are available for consideration, and in all probability, warrant testing and evaluation; however, the two designs studied represented a reasonable choice for the present study. Specifically, they offered relatively high response capability, fabrication simplicity*, low cost of manufacture*, adaptability to pulse mode engine designs where injector heat soak and propellant boiloff problems prevail, and, for one design in particular, relative insensitivity to vibration imposed environments.

The showerhead injector is a flat plate in which orifices of various size (to vary pressure drop) and of various numbers (to vary mass distribution) are drilled. The following criteria were used to design the showerhead injectors:

a. The orifices are located in circular rows.

b. The distance between the chamber wall and the outer orifice row is equal to the spacing between orifices to prevent flow concentration near the walls of the chamber.

c. The orifices cover approximately equal areas of the catalyst bed.

---

* This represents an important factor in the subject program in that numerous injector elements had to be fabricated to support the required thrust level, pressure drop, and injector mass distribution test matrix. Also, the selected designs are readily amenable to characterization and optimization since a large number of variables and tests are not involved.

The rigimesh injector is a modified showerhead type injector in which the local bed loading (bed loading under each orifice) is appreciably less than the injector described above. The rigimesh injector consists of a number of circular rigimesh discs which were press fit into a retaining plate. Each disc was approximately 0.25 inch in diameter. The rigimesh design was selected primarily for its ability to prevent catalyst "fines" and particles from entering the injector and inlet passages under vibration induced environments (spacecraft launch vehicle boost phase loads, for example (Reference 4).

Injector optimization tests included determination of engine ignition delay time, chamber pressure rise time to 80% of steady state value, chamber pressure decay time to 10% of steady state value, chamber pressure roughness, characteristic velocity, specific impulse, and thrust coefficient. In addition, catalyst bed, injector head, and propellant temperature were measured during each test. The techniques used in the data reduction are explained in the ensuing paragraphs.

Ignition delay is defined as the time from entry of propellant into the chamber until the chamber pressure downstream of the catalyst bed undergoes 1% of the change from initial to steady state value. On engine start, the feed pressure (measured just upstream of the propellant valve) drops off momentarily as the ullage volume between the valve and injector is filled. The point at which this pressure begins to rise after dropping off is assumed to be the time when propellant begins to enter into the chamber. A special flow test was conducted to verify that this assumption is approximately correct. This test consisted of placing a conductivity probe underneath one of the injector orifices and measuring the time lapse between feed pressure start rise and closing of the conductivity probe circuit by stream impingement on the probe. This time lapse was at most one (1) millisecond. The ignition delay time thus defined is obtained from the oscillograph record.

Chamber pressure rise time is defined as the time from propellant entry into the chamber to achievement of 80% steady state chamber pressure. The 80% value is taken as a percentage of the steady state chamber pressure downstream of the catalyst bed expressed in absolute units. Rise time to 80% of steady state chamber pressure was selected in lieu of 90% because it appeared to be a more consistent parameter. During the engine testing rise times to 90% chamber pressure average 2.7 times those to 80%. Chamber pressure decay time is defined as the time from downstream chamber pressure start decay to 10% of the steady state value measured in psig units.

Chamber pressure roughness is defined as the peak-to-peak variations in the chamber pressure downstream of the catalyst bed. The data were taken off the oscillograph at a run time between 20 and 30 seconds.

As a first step in determination of the effect of injector variables on performance (cold bed response times, ignition delay, chamber pressure decay time, and chamber pressure roughness) scatter diagrams of the data were plotted. In the scatter diagram each separate factor is plotted without considering any other factor. The scatter diagram points out significant trends without lengthy correlation analysis. Subsequently, statistical tests were made of the data for determination of levels of significance in trends noted from the scatter diagram. If a complete test matrix was completed, a factorial analysis of variance was performed on the data to determine levels of significance and to determine interactions which may exist between the injector variables. When a complete test matrix was not completed, "F" tests were conducted to determine levels of significance.

Details of the injector testing at each thrust level are discussed in Volume I of the subject report. The injector test results reveal certain consistencies in the data at all three thrust levels. The trends and recommended injector design criteria are summarized below.

It was found that cold bed response time increased with increasing injector pressure drop at all three thrust levels. This result appears to be caused by the higher surge flow rates which exist during the start transient for the low pressure drop injectors. Since chamber pressure was held constant for all of the tests, as the injector pressure drop is lowered, the flow resistance decreases resulting in higher transient flow rates. It appears that an increase in propellant input flow rate increases decomposition rate, which suggests that catalyst activity is not the controlling parameter. The data obtained suggests that faster response times can be obtained by increasing the ratio of propellant flow rate to reactor volume. It is noteworthy that the trend of cold bed response with injector pressure drop was observed at each thrust level although the nominal design bed loading increased with thrust level. The effect of bed loading on response time is described further in following sections.

The data obtained with the 5 and 50 lbf engines with the showerhead injector suggest an optimum number of orifices for minimum cold bed response time. Minimum

response times were obtained for both the 5 and 50 lbf engines at approximately 5.3 and 5.6 orifices per square inch of catalyst bed cross sectional area respectively. Apparently minimum response time corresponds to about 6 orifices per square inch of catalyst bed cross sectional area.

With the injector flush with the catalyst bed, smooth start-transient and steady state operation could be obtained with low pressure drop injectors. This indicates that atomization of the propellant is not as critical for the Shell 405 catalyst as for the nonspontaneous catalyst studied by Grant (Reference 3).

Smooth operation is possible with a space between the injector and the catalyst bed. There appears to be no advantage, however, for this arrangement. At the 0.5 and 5 lbf thrust levels ignition delay, chamber pressure response time, and roughness increased when the injector was separated from the catalyst bed. At the 50 lbf thrust level very similar results were obtained with the injector located either flush or 0.25 inches from the catalyst bed.

The rigimesh injector is a workable injector concept and gives performance similar to the showerhead injector with the following exceptions:

a. Chamber pressure oscillations are larger

b. Chamber pressure decay times are longer.

c. The rigimesh injector performance is more sensitive than that of the showerhead injector to distance between the injector and the catalyst bed. This is probably caused by nonaxial flow from the rigimesh elements and the impingement of this flow on the chamber walls.

One of the main advantages of the rigimesh injector is that it offers better resistance than the showerhead injector to plugging by catalyst fines which might be generated by a vibration environment. This is especially true in cases where small orifices are required. One disadvantage of the rigimesh injector is the difficulty in predicting flow characteristics. Prior to detail design of the rigimesh injector, flow tests were conducted on several sizes of rigimesh. It was found that the flow data thus obtained was not consistent with that obtained later when the injectors were manufactured. There are probably two problems which lend to this lack of consistency. One is variation in wire diameter. For the same thickness of rigimesh, marked changes in the flow rate per unit cross sectional area can be

caused. Up to 50% variations have been quoted by the vendor. A second is application of excessive clamping pressure during machining. This can result in decreasing the thickness of the rigimesh and thus reductions in the pore size. If this material is to be used, it must be ordered to produce a given flow rate per unit cross sectional area.

It is felt that the showerhead injector is superior to the rigimesh injector for most applications; it was therefore selected for use in the bed loading, chamber pressure, and bed length phase of the subject program. In most cases orifice diameters can be kept relatively large through the use of low pressure drop injectors. Additionally, reactor operation is not critically dependent on the number of orifices so that the number of orifices can be reduced from the indicated optimum without significant degradation in reactor performance. Orifice sizes as small as 0.010 inches have been used on the program with no sign of orifice plugging.

The following design criteria is recommended for the showerhead injector:

a. Use approximately six orifices per square inch of catalyst bed cross sectional area. If required, this can be reduced by a factor of at least two without serious degradation in engine operation.

b. Utilize low pressure drop injectors. The pressure drop can be held to 10 to 15% of the steady state chamber pressure. It should be noted that an injector pressure drop of 10% of steady state chamber pressure was the lowest value tested in the program.

c. Mount the injector flush (in contact) with the top of the catalyst bed.

d. Propellant can be fed into the injector manifold through a single supply tube. Propellant velocities in the supply tube as high as 50 to 75% of the injector stream velocities were utilized in the study with no adverse effect on propellant distribution and/or reactor operation.

e. Velocity in the propellant distribution manifold as high as 20 to 30% of the injector distribution stream velocities were utilized in the study without having maldistribution of flow to the injector orifices.

f. No evidence was found to indicate that high L/D orifices and turbulent stream characteristics are necessary criteria. It appears that orifice lengths can be dictated by the injector plate thickness needed to meet structural requirements.

Reverse side blank

PRECEDING PAGE BLANK NOT FILMED.

5.0 AMMONIA DISSOCIATION

Ammonia dissociation data were collected during this study for a range of catalyst bed lengths, chamber pressure, and propellant flow rates for the 0.5 lbf nominal thrust engine (diameter = 0.54 inches), the 5 lbf nominal thrust engine (diameter = 1.2 inches), and the 50 lbf nominal thrust engine (diameter = 3.01 inches). The 0.5 lbf engine contained 20-25 mesh granular catalyst throughout the catalyst bed. The 5 lbf engine contained a 0.3 inch layer of 25-30 mesh catalyst near the injector with the remainder of the bed 14-16 mesh, while the 50 lbf engine contained a 0.2 inch layer of 25-30 mesh catalyst at the injector with 1/8" x 1/8" cylindrical pellets in the remainder of the bed. As part of the study, a method was developed to correlate ammonia dissociation data from the engine tests. This method and its application to data collected is discussed in the ensuing paragraphs.

As a first step in analysis of rate data for a heterogeneous chemical reaction, it is usual practice (Reference 8) to determine the importance of the mass transfer resistance associated with diffusion of reactants and products to and from the catalyst surface. For high temperature reactions involving very active catalyst there are some cases where the reaction at the surface approaches chemical equilibrium and diffusion to and from the surface rather than reaction kinetics controls the chemical conversion rate. (This would correspond to an ammonia concentration near zero at the catalyst surface in the present case for the range of pressures and temperatures studied). A specific example of a diffusion controlled reaction is the catalytic decomposition of concentrated hydrogen peroxide (Reference 9).

One method to determine whether or not diffusion is important is to plot measured values of degree of conversion against gas residence time in the catalyst bed for various values of superficial mass velocity (bed loading). If diffusion is important, the degree of conversion at a given residence time (ratio of reactor volume to volumetric flow rate) will increase as the bed loading increases; according to the film theory this results from a decrease in the thickness of the stagnant boundary layer (at the catalyst surface) through which diffusion must occur. If the kinetics of the absorption, surface reaction, or desorption steps were controlling, the conversion at constant residence time would be independent of bed loading.

Figures 7, 8, and 9 are typical plots of data obtained to relate fractional ammonia dissociation to average gas residence time at various values of bed loading. The fractional ammonia dissociation is clearly a function of bed loading at constant residence time; accordingly, diffusion resistance appears to be quite significant for this reaction.

In view of the apparent importance of diffusion during dissociation of ammonia formed by hydrazine decomposition, a relation was developed to relate the fractional ammonia dissociation to temperature, bed loading, and residence time for the limiting case of zero ammonia concentration at the catalyst surface (diffusion of ammonia thereby being rate controlling). This development is described in the following paragraphs.

The general approach to development of a relationship for ammonia dissociation was to:

a. Assume diffusion of ammonia to the catalyst surface is rate controlling (i.e., reaction at the catalyst surface is very fast).

b. Based on the assumption of (a.) above, develop an expression relating fractional ammonia dissociation to catalyst surface area, gas residence time, chamber pressure, and bed loading.

A differential mass of volume of the catalyst bed is shown in Figure 10. Performing an ammonia mass balance on this volume gives:

$$\text{Input} = \text{Output} + \text{Dissociation}$$

$$\frac{GA_b}{\bar{M}} y_{NH_3} \Bigg|_{L} = \frac{GA_b}{\bar{M}} y_{NH_3} \Bigg|_{L+\Delta L} + k_g A_s A_b \left(P_{NH_3} - 0\right) \Delta L \quad (5)$$

Where:

G = Superficial mass velocity, $lbm/in^2\text{-sec}$

A_b = Cross sectional area of catalyst bed, in^2

$\bar{M}$ = Average molecular weight

y_{NH_3} = Mole fraction of ammonia

L = Distance from inlet of catalyst bed, in.

k_g = Mass transfer coefficient, lb/mole-psi-sec-in^3

A_s = Catalyst specific surface area, in^2/in^3 bed

P_{NH_3} = Partial pressure of ammonia in bulk gas stream, psia

But:

$$\bar{M} = \frac{96}{5 + 4X} \tag{6}$$

$$y_{NH_3} = \frac{4(1 - X)}{5 + 4X} \tag{7}$$

$$P_{NH_3} = \frac{4(1 - X)}{5 + 4X} P \tag{8}$$

Where:

X = Fractional ammonia dissociation

P = Total pressure, psia

Substituting equations (6), (7), and (8) into equation (5) and taking the limit as $\Delta L \longrightarrow 0$ gives:

$$\frac{G}{24} \frac{dX}{dL} = 4k_g A_s \frac{(1 - X)}{5 + 4X} P \tag{9}$$

The residence time is defined as the length of the catalyst bed divided by the average velocity of the gases in the catalyst bed and may be expressed as:

$$t = \frac{\epsilon L \bar{M} P (1{,}000)}{G R T} \tag{10}$$

Where:

t = Residence time, milliseconds

ϵ = Volume fraction voids between particles

T = Gas temperature, °R

R = Universal gas constant = 18,528 in lbf/lb mole °R

Differentiating equation (10) and substitution of equation (6) yields:

$$dL = \frac{(5 + 4X)}{96\epsilon} \frac{G R T}{P} dt \qquad (11)$$

Substitution of equation (11) and (9) gives:

$$\frac{dX}{dt} = \frac{k_g A_s R T}{\epsilon} (1 - X) \qquad (12)$$

The form of k_g for the case at hand is (Reference 5):

$$k_g = b_1 \left(\frac{G}{\bar{M} P_f}\right) \left(\frac{\mu}{\rho D_d}\right)^{-2/3} \left(\frac{d_p G}{\mu}\right)^{-0.29} \qquad (13)$$

Where:

b_1 = A constant (determined experimentally)

P_f = A film factor approximately equal to $4P/(3 + X)$

μ = Gas viscosity, lbm/in-sec

ρ = Gas density $\triangleq$ 0.000721 P for present case, lbm/in^3

D_d = Ammonia diffusivity (proportional to $\frac{T^{3/2}}{P}$), in^2/sec

d_p = Diameter of spherical particle which has same volume as volume of particle, ft.

Substitution of equation (13) into (12) and using $D \alpha \frac{T^{3/2}}{P}$ gives:

$$\frac{dX}{dt} = b_2 A_s (1 - X) (3 + X) (5 + 4X) \frac{G^{0.71}}{d_p^{0.29} P} T^2 \qquad (14)$$

Assuming an adiabatic reactor with zero axial conduction, the gas temperature can be expressed as (Reference 3):

$$T \triangleq (1,650 - 780X)\ ^\circ K \qquad (15)$$

Substitution of equation (15) into equation (14) gives the final result as:

$$\int_{X_1}^{X} \frac{dX}{(1 - X)(3 + X)(5 + 4X)(1650 - 780X)^2} = b_2 \frac{A_s}{d_p^{0.29}} \frac{G^{0.71} t}{P} \quad (16)$$

Based on data summarized in Brown (Reference 8), the exponents 0.29 and 0.71 are somewhat particle size dependent for small particles. Also, for particles larger than 1/8 inch the constant b_2 is independent of particle size. For smaller particles there is evidence (Reference 5) that b_1 (and hence b_2) are dependent on particle size.

From equation (16) it is seen that for given particle size and degree of packing, the fractional ammonia dissociation should depend only on the parameter $G^{0.71} t/P$.

For this limiting case the fractional ammonia dissociation for a given catalyst size and degree of packing would depend only on the value of the parameter, $G^q t/P$.

Assuming this limiting case to be a valid first approximation for treating the ammonia dissociation data, the approximate value of q was determined from the experimental data by the following procedure. First, it is noted that at a specified value of X, the quantity should be constant, thus:

$$\frac{G^q t}{P_c} = C$$

$$\ln \frac{t}{P} = -q \ln G + \ln C$$

Accordingly, a plot of ln G versus ln t/P with X held constant should be linear with a slope of (-q). Plots of this type are shown in Figures 11, 12, and 13. The value of q determined in this way is 0.7 for the 0.5, 5, and 50 lbf engines. These values agree closely with values expected on the basis of mass transfer correlations in the literature.

To further test the usefulness of this group as a correlation parameter, the quantity (1 - X) was plotted against $G^{.71} t/P$ using data collected on the 0.5, 5, and 50 lbf engines. These plots are shown in Figures 14 through 16. Although there is some data scatter, the

correlation appears sufficiently good to be useful for design purposes. It is quite possible that additional refinement of this general approach will lead to an improved correlation. For example, no attempt has been made in calculating residence time for ammonia dissociation to make a deduction to account for the volume (or zone) in which hydrazine evaporation and decomposition is occurring. Based on temperature data, it appears that the size of this zone is decreased with both increasing pressure and decreasing bed loading (Grant, Reference 3, found evidence of this same effect). An additional refinement would account for the fact that the bed contains two catalyst zones of difierent particle size. To correct for this, one would first have to estimate the size of the hydrazine evaporation-decomposition zone (perhaps based on temperature data), thereby determining what portion of each catalyst zone is effective for ammonia dissociation. Finally it is conceivable that the pressure dependence of ammonia dissociation would be better described by use of a modified correlating parameter, $G^{.71}\ t/P^r$, where r is empirically determined to give the best possible correlation.

It is emphasized that the use of $G^{.71}\ t/P$ as a correlating parameter is offered here as a useful tool for handling ammonia dissociation data, but not as a proof that the ammonia dissociation is controlled solely by diffusion rate limitations. A preliminary calculation based on estimated diffusion coefficients, a generalized mass transfer correlation, and the assumption of a diffusion controlled reaction gave calculated conversion rates several fold higher than the observed values. Figures 7, 8, and 9, on the other hand, are strong evidence that diffusion is at least a part of the rate controlling mechanism.

Additional work was accomplished to convert the ammonia dissociation data obtained with each catalyst particle size (i.e., thrust level) to a single correlation which includes the effects of particle size.

Examination of the experimental data in Figures 14 through 16 and use of equation (16), suggests that the data from all three engines may possibly be expressed by the following semi-empirical relationship:

$$\ln\left(\frac{1-X_o}{1-X}\right) = K_D\, d_p^{\,m}\, \frac{G^{0.71}\, t}{P} \qquad (17)$$

Where:

X_o = Zero time intercept on plot of experimental data

K_D = An experimentally determined constant

m = An experimentally determined constant

For each engine size a least squares fit was made of the ammonia dissociation data plotted as ln (1 - X) versus $G^{0.71}t/P$. From these curves the value of X_o was determined for each engine size. These values were then averaged to obtain an average value of X_o applicable to all three engine sizes. The average value of X_o thus obtained was 0.5.

Using an average X_o of 0.5, the value of $K_D d_p^m$ was calculated for each engine size again using a least squares technique. The values thus obtained were 480, 425, and 262 for the 0.5, 5, and 50 lbf engines respectively.

For each engine size we then have equations of the form:

$$K_D d_{p_{0.5}}^{\ m} = N_{0.5} \tag{18}$$

$$K_D d_{p_5}^{\ m} = N_5 \tag{19}$$

$$K_D d_{p_{50}}^{\ m} = N_{50} \tag{20}$$

Equations (18), (19), and (20) were solved three ways to determine the values of m and K_D. The average of these three values was then taken to obtain values of m and K_D for equation (17). The values obtained were -0.32 for m and 152.3 for K_D. Using these values equation (17) is expressed as:

$$\ln\left(\frac{1-0.5}{1-X}\right) = 152.3\,\frac{G^{0.71}\,t}{d_p^{\ 0.32_p}} \tag{21}$$

Ammonia dissociation data obtained from all three engines is shown in Figure 17 with ln (1 - X) plotted against $G^{0.71}t/d_p^{\ 0.32_p}$. Although some scatter exists in the correlation, it does appear sufficient for design purposes. Statistical analysis of all of the ammonia dissociation data indicates a 3σ deviation in X of 6% from that given by equation (21).

Reverse Side Blank

PRECEDING PAGE BLANK NOT FILMED.

6.0 CATALYST BED LENGTH REQUIREMENTS

In an ideal adiabatic reactor, the hydrazine decomposition process is commonly described by dividing the catalyst bed into three separate zones. In the first zone, the hydrazine is injected into the catalyst bed and is vaporized. In this zone, part of the hydrazine is also decomposed and supplies part of the heat required for vaporization. In zone two, the remainder of the hydrazine is decomposed. In zone three, partial dissociation of the ammonia occurs. In an actual reactor there are no sharp boundaries which separate the various zones in the catalyst bed. Asymmetries in injection of the liquid hydrazine, the degree of hydrazine atomization, heat losses, wall effects, nonuniformity in packing the catalyst bed, and recirculation of flow in the catalyst bed causes interaction and mixing of the various zones. Little theoretical work has been done studying the bed length requirements for complete hydrazine decomposition and stable reactor operation. Because of the difficulties in treating this problem theoretically, an empirical expression has been developed based on test experience gained in the program wherein satisfactory reactor operation is obtained.

During initial testing on the program on 5 and 50 lbf engines wherein the catalyst bed was composed entirely of 1/8" x 1/8" cylindrical pellets or large mesh size granules, cyclic oscillations in chamber pressure occurred. Tests were made to investigate possible causes of the instability including feed system coppling, insufficient injector pressure drop, and inadequate mass distribution onto the catalyst. None of these had a significant effect on stability. These negative results led to further investigation of the catalyst itself. It was postulated that the instability was caused by flame front oscillations in the catalyst bed and that the surface area of the catalyst was not sufficient to stabilize the flame front near the top of the catalyst bed. This hypothesis was checked by adding various amounts and sizes of fine mesh catalyst at the top of the catalyst bed, thereby providing much higher surface area per unit volume of catalyst bed for the decomposition reaction. Marked reductions in chamber pressure roughness resulted. It was found that approximately 0.2 inch of 25-30 mesh catalyst located at the top of the catalyst bed would produce smooth steady state operation with chamber pressure oscillations not exceeding $\pm$ 2 to $\pm$ 3 percent. It is felt that the fine mesh catalyst acts as a flame holder which establishes and maintains the flame front near the top of the catalyst bed. All subsequent testing conducted during the program employed the 25-30 mesh catalyst on the top of the catalyst bed.

Preliminary analysis and plotting of the data indicated that the data may be correlated by an empirical relationship given by:

$$L_B = 0.2 + \frac{K G^a}{P_c^{\,b} A_s^{\,c}} \qquad (22)$$

Where:

L_B = Minimum bed length, in.

K = A constant determined experimentally

G = Superficial mass velocity, lb/in^2-sec

P_c = Stagnation chamber pressure, psia

A_s = Specific surface area of lower portion of catalyst bed

a = A constant determined experimentally

b = A constant determined experimentally

c = A constant determined experimentally

The bed length required for stable operation was estimated from test data accumulated during the bed loading, chamber pressure, and bed length studies on the 0.5, 5, and 50 lbf engines. It should be noted that some judgment was used in arriving at the bed lengths since tests were not always conducted at exactly the length (L_B) selected.

Equation 22 can be rewritten as:

$$\ln (L_B - 0.2) = \ln \frac{K G^a}{A_s^{\,c}} - b \ln P_c \qquad (23)$$

Thus, for a constant bed loading and catalyst specific surface area, a plot of ln (L_B - 0.2) versus ln P_c will determine the value of the constant b. Figures 18 and 19 present typical plots of the data from the 5 and 50 lbf engines respectively. Linear regression curves were fit through the data for each bed loading condition. The value of b determined for the 0.5 lbf engine was -0.306, for the 5 lbf engine was -0.309, and -0.303 for the 50 lbf engine.

Equation 22 can also be rewritten as:

$$\ln (L_B - 0.2) = \ln \frac{K P_c^{\,b}}{A_s^{\,c}} + a \ln G \qquad (24)$$

Thus, for a constant chamber pressure and catalyst specific surface area, a plot of $\ln (L_B - 0.2)$ versus $\ln G$ will determine the value of the constant a. Figures 20 and 21 present typical plots of the data from the 5 and 50 lbf engines respectively. Again linear regression curves have been fit through the data for each chamber pressure condition. The value of a determined for the 0.5, 5 lbf and 50 lbf engines was 0.558, 0.589, and 0.519, respectively.

Three values for each of the two constants were averaged giving values of -0.306 for b and 0.554 for a. The value of c was determined to be 0.3 using the same techniques as were used in determining the constants a and b.

The value of K in equation 22 was determined to be 145. Thus, the minimum bed length required to obtain stable engine operation can be written as:

$$L_B = 0.2 + \frac{145\, G^{0.554}}{P_c^{\,0.306} A_s^{\,0.3}} \qquad (25)$$

The bed length predicted by this equation is compared to that found experimentally in Figure 22. Good agreement from this equation with that from test data is noted especially in view of the fact that the bed length required from test data was in some cases interpolated between two test points. It should be noted that use of the above equation will result in an ammonia dissociation of approximately 55%.

In summary, for reactors designed for rocket engine applications, it is recommended that the bed length be calculated from Equation 25 with 0.2 inches of 25-30 mesh catalyst being used on the top of the catalyst bed. The catalyst particle size used in the remainder of the bed should be such that the ratio of reactor diameter to particle size diameter is at least 8:1 (Reference 10) so that wall effects and possible channeling of flow in the catalyst bed are minimized. It should also be noted that the bed loading and/or chamber pressure selected should never be such that the catalyst bed pressure drop is greater than 40 psid (see Section 7.0).

Reverse Side Blank

PRECEDING PAGE BLANK NOT FILMED

7.0 CATALYST BED PRESSURE DROP

The pressure drop for flow of hydrazine decomposition gas products through the catalyst bed is an important design consideration. It is desirable to limit this pressure loss to: 1) minimize injection pressure and therefore the feed system weight required for a given chamber pressure, and 2) to prevent forces sufficient to cause packing and/or crushing of the catalyst bed.

The pressure loss for flow of fluids through uniform cross-section is correlated by means of the dimensionless Fanning equation as (Reference 11):

$$\Delta P = \frac{2f G^2 L}{g_c D_c \rho} \tag{26}$$

The dimensionless friction factor f is correlated as a function of the Reynolds Number and cross-section roughness.

For flow through packed beds, the Fanning equation must be modified to include terms for the effective cross-sectional area available for flow and for the effective hydraulic radius of the path between particles. These modifications are strongly dependent on the method of packing the catalyst bed. If the catalyst is poured in a continuous manner into the chamber, a loose packing arrangement is obtained with a large void volume in the bed, which is referred to as a random loose arrangement. Conversely, if the catalyst is added to the chamber such that each particle falls to rest before another falls on top of it, a high bulk density results; this leads to what is termed a random dense arrangement. Several factors of difference can exist in pressure drop between the two packing arrangements. Since from a reactor design standpoint it is more efficient to utilize a random dense packing, such a packing technique was utilized in this study.

Oman and Watson (Reference 12) proposed the following equation for correlation of pressure losses in packed beds whose packing was a random dense arrangement:

$$\Delta P = \frac{2 f_d G^2 A_s L}{\rho g_c \epsilon^{1.7}} \tag{27}$$

Where:

ΔP = Catalyst bed pressure drop, psid

f_d = Friction factor

A_s = Catalyst specific surface area, in^2/in^3

G = Superficial bed loading, lbm/in^2-sec

L = Catalyst bed length, in

ρ = Average gas density, lbm/in^3

g_c = Gravitational constant

ϵ = Catalyst bed porosity

The dimensionless friction factor, f_d, was correlated by means of a modified Reynolds Number, N_r, which is defined as:

$$N_r = \frac{G}{\mu A_s}$$

Where:

μ = Average gas viscosity, lbm/in-sec (Approximately 1.75×10^{-6})

When the friction factor is plotted against Reynolds Number on log-log paper, a smooth curve of gradually changing slope is obtained which is approximated by two straight lines as (Reference 12):

$$f_d = \frac{2.6}{N_r^{0.3}} \qquad 10 < N_r < 150$$

$$f_d = \frac{1.23}{N_r^{0.15}} \qquad 150 < N_r < 300$$

The above equation has limited applicability because the range of Reynolds Numbers of interest for monopropellant hydrazine reactors goes as high as 3,000. Grant, in his work with the nonspontaneous catalyst (Reference 3), assumed the friction factor could be expressed as:

$$f_d = K N_r^f$$

Thus, equation (27) was expressed as:

$$\Delta P_c = K \frac{A_s^{1-f}}{F_v^{1.7}} G^{2+f} \frac{L_c}{\rho_c} \qquad (28)$$

The work conducted by Grant determined the following values for the constants in equation (28):

$f = -0.2$ $\quad$ $100 < N_r < 600$

$K = 1260$

$f = 0$ $\quad$ $600 < N_r < 3000$

$K = 3900$

Another equation frequently used in estimating pressure drop through packed beds is the Ergun equation (Reference 13) developed from combining the Blake-Kozeny equation for laminar flow and the Burke Plummer equation for highly turbulent flow. This equation is expressed as:

$$\Delta P = N_r^1 (\alpha + \beta N_r^1) \frac{\mu^2}{g_c \rho d_p^3} \left(\frac{1-\epsilon}{\epsilon} \right)^3 L \qquad (29)$$

Where previously undefined terms are:

N_r^1 = Modified Reynolds Number = $\frac{G d_p}{\mu(1-\epsilon)}$

α = An experimentally determined constant = 150

β = An experimentally determined constant = 1.75

d_p = Diameter of a spherical particle which has the same volume as volume of particle, in

Experimental pressure drop data from the study was compared with that predicted by the Oman and Watson equation, by Grant's equation, and by the Ergun equation to see if these equations adequately predicted the measured catalyst bed pressure drop. Test conditions covered Reynolds Numbers of 35 to 2500, and catalyst particle sizes ranging from 25-30 mesh

granules to 1/8" x 1/8" cylindrical pellets. Figure 23 is a plot of experimentally measured catalyst bed pressure drop versus that calculated by Grant's or the Oman-Watson equation for data from the 0.5, 5, and 50 lbf engines. The agreement between the experimental data and that predicted by Grant's equation is good with maximum data scatter being ±20% of the predicted values.

Figure 24 presents correlation of the data from the 0.5 and 5 lbf engines versus that predicted from the Ergun equation. Comparable agreement to Grant's equation is obtained with the Ergun equation for the 0.5 and 5 lbf engines. However, the Ergun equation predicts significantly higher pressure drops than those measured on the 50 lbf engine. The Ergun equation appears to give calculated values of pressure drop close to those measured for modified Reynolds Numbers less than 2,000, but at higher Reynolds Numbers (as encountered on the 50 lbf engine), the equation does not adequately predict the measured pressure drop.

Testing conducted on the program covered catalyst bed pressure drops as high as 75 psid with no catalyst breakup being noted. However, some additional settling and packing of the bed did occur under these conditions. Based on the experience gained in this study, it is recommended that the catalyst bed be designed for pressure drops not exceeding 40 psid.

8.0 CHAMBER PRESSURE RESPONSE TIME

The pressure response time may be defined as the time, measured from the time of the propellant valve actuation signal, required to reach an arbitrary fraction of steady state chamber pressure. Response time thus defined is affected by (1) the valve response characteristics, (2) the feed line hydraulic delay (time for propellant to flow from the propellant valve to the injector), (3) the ignition delay (time to wet the catalyst and for initial decomposition heat release to bring some catalyst particles to a temperature at which the decomposition is rapid), and (4) the pressure rise delay time (time to decompose enough hydrazine to fill the void space in the reactor and heat up the entire catalyst bed).

Valve response characteristics and feed line hydraulic delay were not specifically studied in this program. However, an effort was made to minimize their effect so as to allow reproducible measurement of ignition delay and pressure rise times. The valves used in this program had an opening time of approximately 15 millisceconds. The distance between the valve and injector was minimized within the constraints imposed by need to control heat soak to the propellant valve.

Ignition delay and pressure rise times were measured in all tests. No specific correlation was obtained for ignition delay time, but with proper injector design the measured ignition delay was found to be approximately 10 to 20 milliseconds for catalyst and hydrazine temperatures in the range of 40 to 70°F. Pressure rise time is a much larger fraction of the response time for the range of experimental variables considered in the study.

In the subsequent paragraphs the results of the development of an analytical model for the pressure rise process are described. The analytical approach basically amounts to first assuming complete decomposition during the start transient and then empirically modifying the model thus generated to account for kinetic effects (i.e., rate limitations imposed by propellant atomization process and/or decomposition reaction kinetics).

Pressure rise time is defined herein as the time for chamber pressure measured downstream of the catalyst bed to change from 1% of the steady state value to some specified higher percentage of the steady state pressure. An analytical model of the pressure rise transient was developed by treating the pressure rise transient as a two-stage process. Stage 1 is treated as an isothermal pressurization process in which the accumulation

of gas in the reactor void space is the predominant factor. The system temperature is assumed to be constant at the initial catalyst temperature during this relatively short portion of the pressure rise period. During Stage 2 the catalyst bed heatup as it affects the temperature of gas entering the nozzle is considered to be the predominant factor; as the gas heats up, the chamber pressure rises because of attendant increase in "flow resistance" for gas outflow. The accumulation of gas mass in the reactor is neglected during Stage 2. The details of the analytical approach for both Stage 1 and 2 are covered in the ensuing paragraphs.

The following basic assumptions are made for the development of the Stage 1 phase of the pressure rise model development:

a. Initially it is assumed that all of the input propellant decomposes at the inlet end of the catalyst bed. The result thus obtained is then multiplied by a correction factor to account for kinetic effects.

b. During Stage 1, the temperature of the entire reactor remains constant at the initial catalyst temperature.

c. The ideal gas law applies and the gas molecular weight is constant during Stage 1.

d. The injector orifice discharge coefficient is constant throughout the start transient at the value corresponding to steady state operation.

e. The exit nozzle is assumed choked throughout the start transient with a discharge correction factor equal to that for steady operation.

f. The pressure drop through the catalyst bed is assumed to be given by the Ergun equation (i.e., pressure drop is assumed directly proportional to mass flow rate squared and inversely proportional to gas density.

g. As an approximation the entire void volume to be pressurized including void space between catalyst particles is considered to be concentrated downstream of the catalyst bed. It is clear that a more accurate approach would be to use the pressure drop relation in differential form and write an unsteady state mass balance about a differential volume element, thereby taking into account accumulation within the catalyst bed. However, this more complex approach was not felt justified at this stage of model development. It can be added as a refinement later if desired.

h. Propellant feed pressure is assumed constant throughout the start transient.

A mass balance is written around Volume 1 of Figure 25 neglecting accumulation in the void space between particles (this accumulation is taken into account later by considering it to occur downstream of the catalyst bed). The propellant injection rate is:

$$\dot{m}_i = K_1 \sqrt{P_f - P_{cu}} \tag{30}$$

Where:

$\dot{m}_i$ = Propellant injection rate, lbm/sec

K_1 = A constant dependent on orifice design

P_f = Propellant feed pressure, lbf/in^2

P_{cu} = Chamber pressure upstream of the catalyst bed (i.e., at the injector), lbf/in^2

The catalyst bed pressure drop-flow rate relation (Ergun equation) is:

$$P_{cu} - P_{cd} = K_2 \frac{\dot{m}_b^2 T_{co}}{\bar{M}_1 \bar{P}_c}$$

Where:

$\dot{m}_b$ = Propellant flow rate through the catalyst bed, lbm/sec

K_2 = A constant determined by catalyst particle size and catalyst bed void fraction

T_{co} = Initial catalyst temperature (assumed equal to the gas temperature during Stage 1), °R

$\bar{P}_c$ = Average chamber pressure $(P_{cu} + P_{cd})/2$

P_{cd} = Chamber pressure downstream of the catalyst bed, lbf/in^2

$\bar{M}_1$ = Average molecular weight decomposition products lb/lb mole.

A mass balance around Volume 1 of Figure 25 neglecting accumulation is:

$$\dot{m}_i = \dot{m}_b$$

$$K_1 \sqrt{P_f - P_{cu}} = \sqrt{\frac{\bar{M}_1}{K_2 T_{co}} (P_{cu} - P_{cd}) \bar{P}_c} \tag{31}$$

If the bed pressure drop is not a large fraction of average chamber pressure, then

$$\frac{P_{cu} - P_{cd}}{P_{cd}} << 1 \text{ and } \bar{P}_c \doteq P_{cd}$$

and Equation 31 becomes:

$$K_1^2 (P_f - P_{cu}) = \frac{\bar{M}_1}{K_2 T_{co}} (P_{cu} - P_{cd}) P_{cd} \tag{32}$$

The same mass balance applied to steady state operation gives:

$$K_1^2 (P_f - P_{cu\,\infty}) = \frac{\bar{M}_\infty}{2K_2 T_{c\,\infty}} (P_{cu\,\infty} - P_{cd\,\infty}) P_{cd\,\infty} \tag{33}$$

The ratio of Equations 32 and 33 may be arranged to give:

$$\frac{P_{cu}}{P_{cd\,\infty}} = \frac{FZ(D-1) + (F-D)\eta^2}{Z(D-1) + (F-D)\eta} \tag{34}$$

Where:

$F = P_f / P_{cd}$ (feed ratio)

$Z = M_\infty T_{co} / M_1 T_c$

$D = P_{cu} / P_{cd}$ (catalyst bed pressure drop ratio)

$\eta = P_{cd} / P_{cd\,\infty}$ (fractional approach of downstream chamber pressure to steady state)

A mass balance about Volume 2 depicted in Figure 25 gives:

$$\dot{m}_b = \dot{m}_o + \frac{dm}{dt} \tag{35}$$

Where:

$\dot{m}_o$ = Mass flow rate of gas through the nozzle, lbm/sec

$\frac{dm}{dt}$ = Rate of accumulation of mass in the volume to be pressurized, lbm/sec

Or since $\dot{m}_b = \dot{m}_i$

$$\dot{m}_i = \dot{m}_o + \frac{dm}{dt} \tag{36}$$

Now, assuming a choked nozzle, the outflow is of the form

$$\dot{m}_o = K_3 \sqrt{\frac{\bar{M}_1}{T_{co}}} P_{cd} \tag{37}$$

The accumulation term assuming ideal gas behavior and constant temperature is:

$$\frac{dm}{dt} = \frac{\bar{M}_1 V_c}{RT_{co}} \frac{d P_{cd}}{dt} \tag{38}$$

Where:

V_c = Volume to be pressurized, in^3

R = Gas constant = 18,528 in lbf/lb mole °F

t = Time, measured from the start of Stage 1

Now substitution of Equations 30, 37, and 38 into 36 gives:

$$K_1 \sqrt{P_f - P_{cu}} = K_3 \sqrt{\frac{\bar{M}_1}{T_{co}}} P_{cd} + \frac{\bar{M}_o V_c}{RT_{co}} \frac{d P_{cd}}{dt} \tag{39}$$

The steady state propellant flow rate is:

$$\dot{w}_\infty = K_1 \sqrt{P_f - P_{cu\,\infty}} \quad K_3 \sqrt{\frac{\bar{M}_\infty}{T_{c\,\infty}}} P_{cd\,\infty} \tag{40}$$

Division of Equation 39 by 40 gives:

$$\sqrt{\frac{F - \frac{P_{cu}}{P_{cd\,\infty}}}{F - D}} = \sqrt{\frac{1}{Z}}\eta + \frac{\bar{M}_o V_c P_{cd\,\infty}}{\dot{w}_\infty R T_{co}} \frac{d\eta}{dt} \tag{41}$$

Substitution of Equation 34 into 41 results in:

$$\sqrt{\frac{(F - \eta)\eta}{(F - D)\eta + (D-1)Z}} = \sqrt{\frac{1}{Z}}\eta + \frac{\bar{M}_o V_c P_{cd\,\infty}}{\dot{w}_\infty R T_{co}} \frac{d\eta}{dt} \tag{42}$$

Integrating Equation 42 and employing a correction factor to account for vaporization and/or reaction rate effects results in:

$$t_1 = \frac{K_{c1} \bar{M}_1 V_c P_{cd\,\infty}}{\dot{w}_\infty R T_{co}} \int_{\eta_o}^{\eta_1} \frac{d\eta}{\sqrt{\frac{(F - \eta)\eta}{(F - D)\eta + (D - 1)Z}} - \sqrt{\frac{1}{Z}}\eta} \tag{43}$$

Where:

t_1 = Time for completion of Stage 1, sec

η_o = Value of $P_{cd}/P_{cd\,\infty}$ at the end of the ignition delay

η_1 = Value of $P_{cd}/P_{cd\,\infty}$ at the end of Stage 1 (See Equation 54)

K_{c1} = A correction factor (to be empirically determined) to account for the fact that not all of the propellant input is decomposed during the start transient

The following basic assumptions are made for development of Stage 2:

a. The entire catalyst bed is at a uniform temperature which increases with time and which equals the instantaneous gas temperature leaving the catalyst bed.

b. Gas accumulation in the reactor is assumed negligible (i.e., input flow rate of liquid propellant equals output flow rate of gaseous products during all of Stage 2).

c. The gas molecular weight is assumed constant at an average value during Stage 2.

d. The injector orifice discharge coefficient is assumed constant at the value corresponding to steady state operation.

e. The exit nozzle discharge correction factor is assumed constant at the value obtained for steady state operation.

f. The pressure drop through the catalyst bed is assumed to be given by the Ergun equation.

g. The propellant feed pressure is assumed constant.

h. The propellant is assumed to completely decompose at the injector end of the catalyst bed. A correction is then used to account for incomplete decomposition during the start transient.

From injector flow rate catalyst bed pressure drop, and nozzle flow relationships, the following relationship may be written:

$$\dot{w} = K_1\sqrt{P_f - P_{cu}} = K_4\sqrt{\frac{P_{cu}^2 - P_{cd}^2}{T_c}} = K_5\frac{P_{cd}}{\sqrt{T_c}} \qquad (44)$$

Where:

K_4 = A constant dependent on the particle size and void volume in the catalyst bed

K_5 = A constant

T_c = Catalyst bed and gas temperature, °R

The same relation applied to steady state is:

$$\dot{w}_\infty = K_1\sqrt{P_f - P_{cu\,\infty}} = K_4\sqrt{\frac{P_{cu\,\infty}^2 - P_{cd\,\infty}^2}{T_{c\,\infty}}} = K_5\frac{P_{cd\,\infty}}{\sqrt{T_{c\,\infty}}} \qquad (45)$$

Combining Equations 44 and 45 leads to the following relation between P_{cu} and P_{cd}:

$$\frac{P_{cu}}{P_{cd\,\infty}} = D\eta \tag{46}$$

An approximate energy balance around Volume 3 of Figure 26 is, assuming complete decomposition of all input propellant and thermal equilibrium between the decomposition gases and the catalyst bed:

$$C_c \frac{dT_c}{dt} = \left[\Delta H_{rf} - \bar{C}_{pg}(T_c - T_f)\right] \dot{w} \tag{47}$$

Where:

C_c = Catalyst heat capacity, Btu/°F

ΔH_{rf} = Heat of reaction of hydrazine at the propellant feed temperature

$\bar{C}_{pg}$ = Mean heat capacity of constant pressure of gaseous decomposition products, assumed constant at an average value for the heatup Btu/lbm-°F

T_f = Propellant feed temperature, °F

Equation 47 may be put in dimensionless form by dividing by $T_{c\,\infty}$ and by using Equations 44 and 45 in the form:

$$\dot{w} = \dot{w}_\infty \sqrt{F - (P_{cu}/P_{cd})/(F - D)}.$$

Doing this and then utilizing the relation $\Delta H_{rf} = \bar{C}_{pg}(T_{c\,\infty} - T_f)$, one obtains:

$$\frac{d\theta}{d\tau} = \left[1 - \theta\right] \sqrt{\frac{F - \dfrac{P_{cu}}{P_{cd\,\infty}}}{F - D}} \tag{48}$$

Where:

$\theta = T_c/T_{c\,\infty}$

$\tau = \dfrac{\bar{C}_{pg}\,\dot{w}_\infty\, t}{C_c}$

Now both θ and $P_{cu}/P_{cd\,\infty}$ can be eliminated from this equation in order to relate η to time. Division of Equation 44 by Equation 45 gives:

$$\theta = \frac{(F - D)\eta^2}{F - \dfrac{P_{cu}}{P_{cd\,\infty}}} \tag{49}$$

Substitution of Equation 46 into Equation 49 yields:

$$\theta = \frac{(F - D)\eta^2}{F - D\eta} \tag{50}$$

The derivative of Equation 50 is:

$$\frac{d\theta}{d\tau} = \frac{(F - D)\left[2F - D\eta\right]\eta\,\dfrac{d\eta}{d\tau}}{(F - D\eta)^2} \tag{51}$$

Combination of Equations 50, 51, and 48 followed by integration gives:

$$\tau = (F - D)^{3/2} \int_{\eta_1}^{\eta} \frac{(2F - D\eta)\,\eta\, d\eta}{(F - D\eta)^{3/2}\left[F - D\eta - (F - D)\eta^2\right]} \tag{52}$$

Now, rewriting τ in terms of the original variables and employment of a correction factor K_{c2} to account for decomposition kinetics gives the final result:

$$t_2 = K_{c2}\frac{C_c(F - D)^{3/2}}{\bar{C}_{pg}\,\dot{w}_{\infty}} \int_{\eta_1}^{\eta} \frac{(2F - D\eta)\,\eta d\,\eta}{(F - D\eta)^{3/2}\left[F - D\eta - (F - D)\eta^2\right]} \tag{53}$$

The start of Stage 2 occurs when η reaches η_1, the value of η from Equation 50 which corresponds to the initial catalyst temperature. Accordingly,

$$\eta_1 = -\frac{D\,T_{co}}{2(F - D)T_{c\,\infty}} + \frac{1}{2}\sqrt{\left[\frac{D\,T_{co}}{(F - D)T_{c\,\infty}}\right]^2 + \frac{4F\,T_{co}}{(F - D)T_{c\,\infty}}} \tag{54}$$

The value of η_1 varies somewhat depending on the test conditions. However, to avoid complexities of varying η_1 in determination of the constant, K_{c1}, an average value of 0.8 was assumed.

As a first step in the determination of the value of the constant K_{c1} in the Stage 1 pressure rise model, the integral was evaluated for a wide range of the variables F & D. A typical plot of this integral for varying F and D is shown in Figure 27. For each test conducted, the value of F and D were calculated. Use of Figure 27 then allowed determination of the integral for each test point.

Using test data, the value of $\bar{M}_1 K_{c1}$ was determined for each test from:

$$\bar{M}_1 K_{c1} = \frac{t_1 \dot{w}_\infty R T_{co}}{V_c P_{d_\infty}} \cdot \frac{1}{\int_{\eta_o}^{0.8} \frac{d\eta}{\sqrt{\frac{(F-\eta)\eta}{(F-D)\eta + Z(D-1)}}} - \eta\sqrt{\frac{1}{Z}}}$$

Values of the constant thus obtained were then plotted as a function of inlet feed pressure, chamber pressure and engine pressure drop to see if a correlation existed with any of these parameters. Such plots were made for each engine size and for varying values of Z from 0.5 to 0.7. It was found that $\bar{M}_1 K_{c1}$ was rather insensitive to Z and a value of 0.6 was used. When plotted on log-log paper the constant $\bar{M}_1 K_{c1}$ was a straight line function of chamber pressure for chamber pressures of 225 to 1,000 psia. At chamber pressures of 100 psia and below the experimental value of $\bar{M}_1 K_{c1}$ was higher than that predicted by extrapolating the straight line function obtained at higher chamber pressures. It is strongly suspected that this discrepancy is a result of subsonic flow through the nozzle for an appreciable portion of the pressure rise time at chamber pressures of 100 psia and below. For this reason only test data at chamber pressures between 225 and 1,000 psia was used in determining the value of $\bar{M}_1 K_{c1}$.

A plot of the constant, $\bar{M}_1 K_{c1}$ versus chamber pressure is shown in Figure 28 for the 0.5, 5, and 50 lbf engines. A linear regression curve was fit through the data shown in Figure 28. It is noted that the data obtained from all three thrust levels can be adequately fit by a single curve. The relationship between $\bar{M}_1 K_{c1}$ and chamber pressure thus obtained was:

$$\bar{M}_1 K_{c1} = \frac{3.69 \times 10^4}{P_{d\infty}}$$

Thus the equation for the Stage 1 pressure rise time (time to 80% steady state chamber pressure) is given by:

$$t_1 = \frac{3.69 \times 10^4 V_c}{\dot{w}_\infty R T_{co}} \int_{0.01}^{0.8} \frac{d\eta}{\sqrt{\frac{(F-\eta)\eta}{(F-D)\eta + Z(D-1)}} - \eta\sqrt{\frac{1}{Z}}} \qquad (55)$$

As a first step in the evaluation of the Stage 2 constant, K_{c2}, the integral was evaluated for a wide range of the variables F and D with the integral evaluated between $\eta = 0.8$ and $\eta = 0.9$. Plots of this integral were then made as a function of F and D. This plot is shown in Figure 29. For each test the integral was then evaluated by use of the above plots.

Using the test data, the value of $K_{c2}/\bar{C}_{pg}$ was evaluated for each test from:

$$\frac{K_{c2}}{\bar{C}_{pg}} = \frac{\dot{w}_\infty t_2}{C_c (F-D)^{3/2}} \int_{0.8}^{0.9} \frac{1}{\frac{(2F - D\eta)\eta\, d\eta}{(F-D\eta)^{3/2}\left[F - D\eta - (F-D)\eta^2\right]}}$$

Values of the constant thus obtained were plotted as a function of inlet feed pressure, chamber pressure, and engine pressure drop to see if a correlation existed with any of these parameters. Such plots were made for each engine size. When plotted on log-log paper (Figure 30) the constant $K_{c2}/\bar{C}_{pg}$ was a straight line function of feed pressure. A linear regression curve was fit through the data shown in Figure 30. It is noted that the data obtained at all three engine sizes can be adequately fit by a single curve. The relationship between $K_{c2}/\bar{C}_{pg}$ and feed pressure thus obtained is:

$$\frac{K_{c2}}{\bar{C}_{pg}} = \frac{570}{P_f}$$

Thus the equation for the Stage 2 pressure rise time is given by:

$$t_2 = \frac{570\,(F - D)^{3/2}}{\dot{w}_\infty P_f} \int_{0.8}^{\eta} \frac{(2F - D\eta)\,\eta\, d\eta}{(F - D\eta)^{3/2}\left[F - D\eta - (F - D)\eta^2\right]} \qquad (56)$$

9.0 APPLICATION OF EQUATIONS TO REACTOR DESIGN

The following paragraphs describe the application of design and scaling formulae to design of monopropellant hydrazine rocket engines and gas generators employing Shell 405 spontaneous catalyst.

9.1 Rocket Engine Design

In the design of monopropellant hydrazine reactors it is desirable to limit the ammonia dissociation and thus maximize engine performance. As a starting point in the engine design, it is assumed that previous system analysis has defined engine thrust level and chamber pressure.

Engine propellant flow rate can be calculated from the known thrust level and an estimated delivered specific impulse. Use of a delivered specific impulse 95% of the theoretical value for an ammonia dissociation of 55% is usually sufficient for initial design purposes. Thus:

$$\dot{w} = \frac{F}{0.95\, I_{s_{th}}}$$

The next step in engine design is determination of the engine bed loading (propellant flow rate per unit cross sectional area of the catalyst bed) and the catalyst particle size. This is an iterative procedure because of the interdependence of the variables involved in the calculations. The upper 0.2 inch of the catalyst bed should consist of 25-30 mesh granular catalyst pellets for stability reasons. The catalyst size for the remainder of the bed should be selected such that the ratio of chamber diameter to particle size is approximately 8:1 to 10:1 so that channeling of flow in the catalyst bed is minimized or avoided. For reactors larger than 1.5 inches in diameter, 1/8" x 1/8" cylindrical pellets may be used in the catalyst bed since this is the largest pellet size currently available from the Shell Development Company (November, 1966).

A convenient procedure which may be used to determine engine bed loading and catalyst size requirements is as follows:

a. Arbitrarily choose a bed loading (approximately 0.04 lbm/in^2-sec)

b. Calculate the chamber diameter from:

$$D_b = \sqrt{\frac{4}{\pi} \frac{\dot{w}}{G}}$$

c. Estimate required particle size for the lower portion of the catalyst bed assuming a ratio of chamber diameter to particle diameter of 8:1 to 10:1.

d. Calculate the catalyst bed length required from the following equation:

$$L_B = 0.2 + 145 \frac{G^{0.554}}{P_c^{0.306} A_s^{0.3}}$$

e. Calculate the Reynolds Number of the gas flow through the catalyst bed from:

$$N_r = 5.41 \times 10^5 \frac{G}{A_s}$$

f. Calculate the catalyst bed pressure drop using the equation which fits the Reynolds Number of interest as determined from (e) above.

$$\Delta P = \frac{2 f_d G^2 A_s L}{\rho g_c \epsilon^{1.7}} \qquad 10 < N_r < 100$$

$$\Delta P = \frac{1260 A_s^{1.2} G^{1.8} L}{\epsilon^{1.7} \bar{P}_c} \qquad 100 < N_r < 600$$

$$\Delta P = \frac{3900 A_s G^2 L}{\epsilon^{1.7} \bar{P}_c} \qquad 600 < N_r < 3000$$

Note that the pressure drop must be calculated for both the upper portion of the catalyst bed (25-30 mesh granules) and the lower portion of the catalyst bed. Catalyst bed porosity and catalyst specific surface area may be estimated from data in Section 3.0.

g. Iterate the above procedure returning to Step a. until the catalyst bed pressure drop is 30 to 40 psid. This is the maximum catalyst bed pressure drop recommended for engine design purposes.

Use of the above procedure will result in determination of catalyst bed loading and thus chamber diameter, catalyst particle size, and catalyst bed length. It should be noted that there are some applications where bed loadings less than those calculated from the above procedure may be utilized. Catalyst bed loss rates can be offected by the bed loading employed. Thus, for extremely long engine life, lower bed loadings may be chosen and utilized based mainly on experience and experimental test data. An example of a typical engine design using the above criteria is covered in Appendix I.

9.2 Gas Generator Design

In the design of monopropellant hydrazine reactors for gas generator application it is usually desirable to maximize ammonia dissociation resulting in lower gas temperatures and molecular weight of the gas products. As a starting point in the gas generator design, it is assumed that the gas generator flow rate, chamber pressure and desired ammonia dissociation (i.e., gas temperature and gas product molecular weight) are known and specified. The same design procedure as used for rocket engine design is then employed, except that the catalyst bed length is calculated from Equation (22) in Section 6.0 instead of using the equation for minimum catalyst bed length requirements.

The design procedure is thus as follows:

a. Arbitrarily choose a bed loading

b. Calculate the chamber diameter from

$$D_b = \sqrt{\frac{4}{\pi} \frac{\dot{w}}{G}}$$

c. Estimate required particle size for the lower portion of the catalyst bed assuming a ratio of chamber diameter to particle diameter in the range of 8:1 to 10:1.

d. Calculate the catalyst bed length from the following equation:

$$\ln\left(\frac{1-0.5}{1-X}\right) = 152.5\ \frac{G^{0.71}\ t}{d_p^{0.32}\ P}$$

e. Calculate the Reynolds Number of the gas flow through the catalyst bed from:

$$N_r = 5.41 \times 10^5\ \frac{G}{A_s}$$

f. Calculate the catalyst bed pressure drop using the equation which fits the Reynolds Number range of interest as determined from (e) above.

$$\Delta P = \frac{2 f_d G^2 A_s L}{\rho g_c \epsilon^{1.7}} \qquad 10 < N_r < 100$$

$$\Delta P = \frac{1260 A_s^{1.2} G^{1.8} L}{\epsilon^{1.7}\ \bar{P}_c} \qquad 100 < N_r < 600$$

$$\Delta P = \frac{3900 A_s G^2 L}{\epsilon^{1.7}\ \bar{P}_c} \qquad 600 < N_r < 3000$$

g. Iterate the above procedure until the catalyst bed pressure drop is 30 to 40 psid. This is the maximum catalyst bed pressure drop recommended for reactor design purposes.

Use of the above procedure will then result in determination of the catalyst bed size and catalyst pellet size required to meet the gas generator design requirements. An example of a typical gas generator design is contained in Appendix II.

HYDRAZINE PERFORMANCE CURVES (100% N_2H_4)

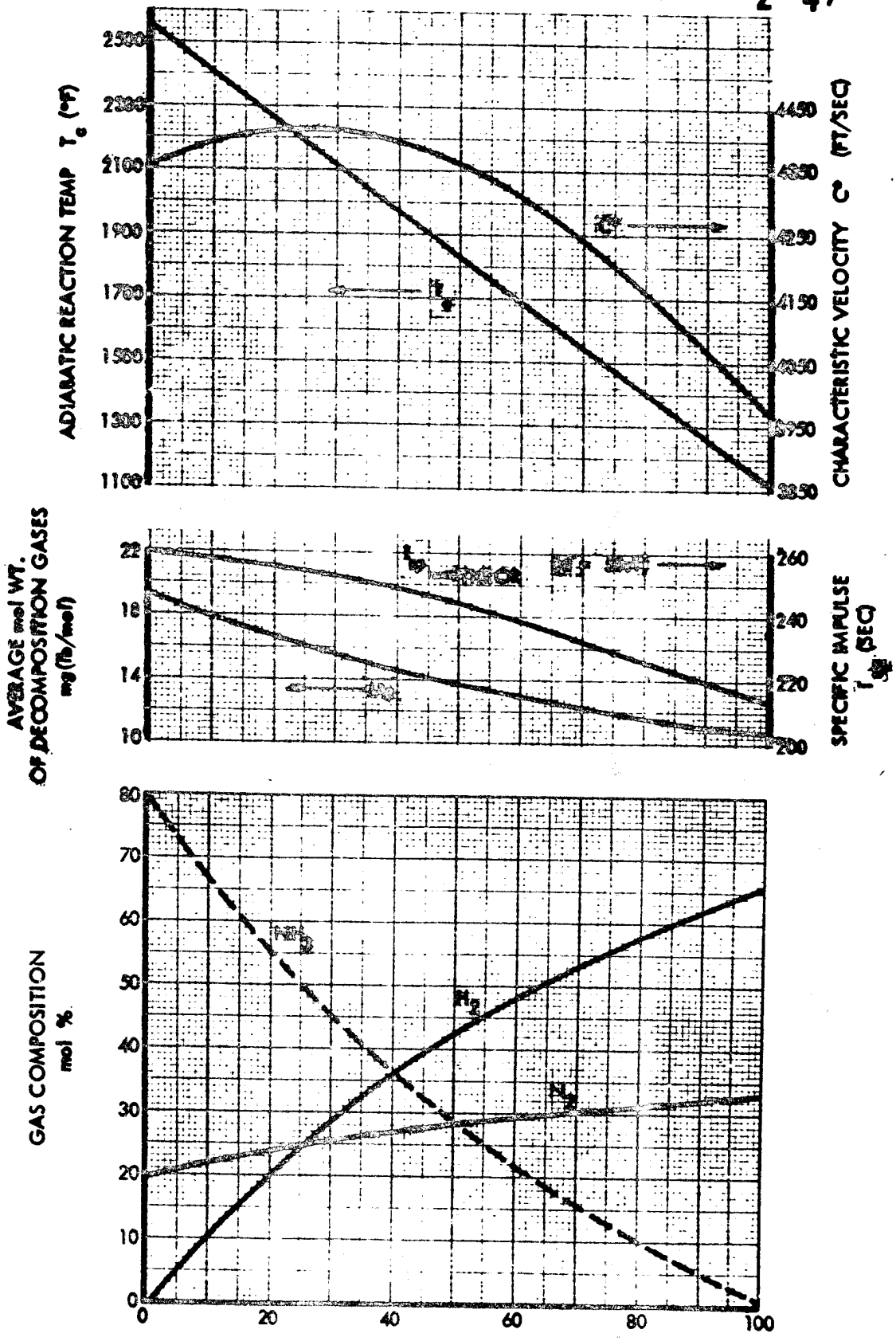

FIGURE 1

CATALYST BED POROSITY VS CATALYST BED DIAMETER FOR 1/8" x 1/8" CYLINDERS

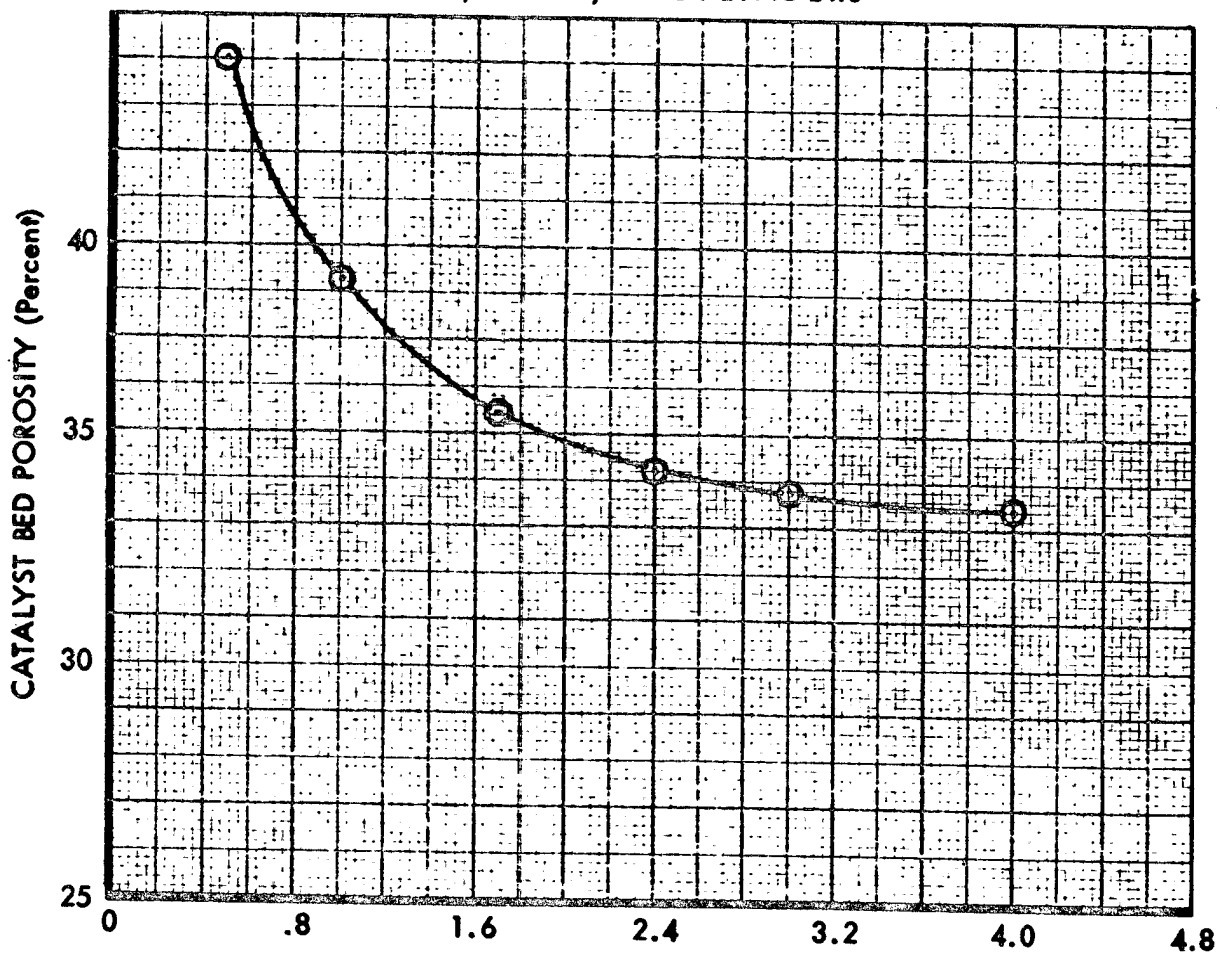

SPECIFIC SURFACE AREA VS CATALYST BED DIAMETER FOR 1/8" x 1/8" CYLINDERS

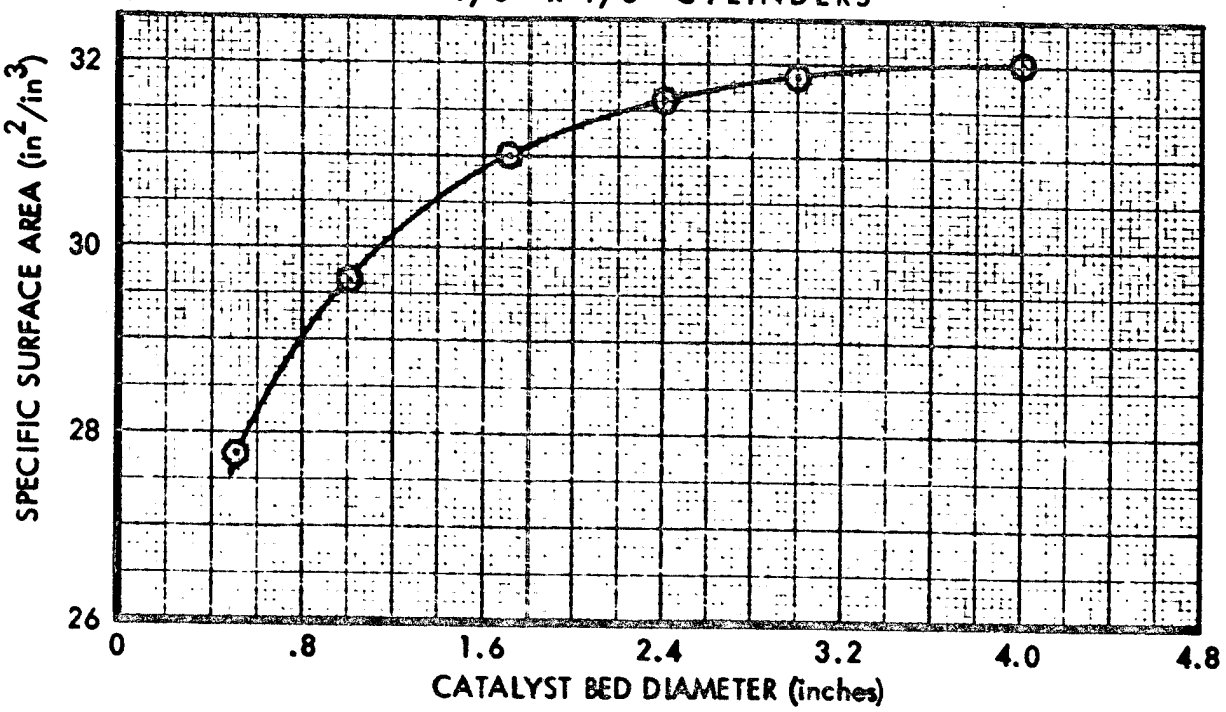

11779

FIGURE 2

CATALYST BED POROSITY VS CATALYST BED DIAMETER FOR 1/8" x 1/16" CYLINDERS

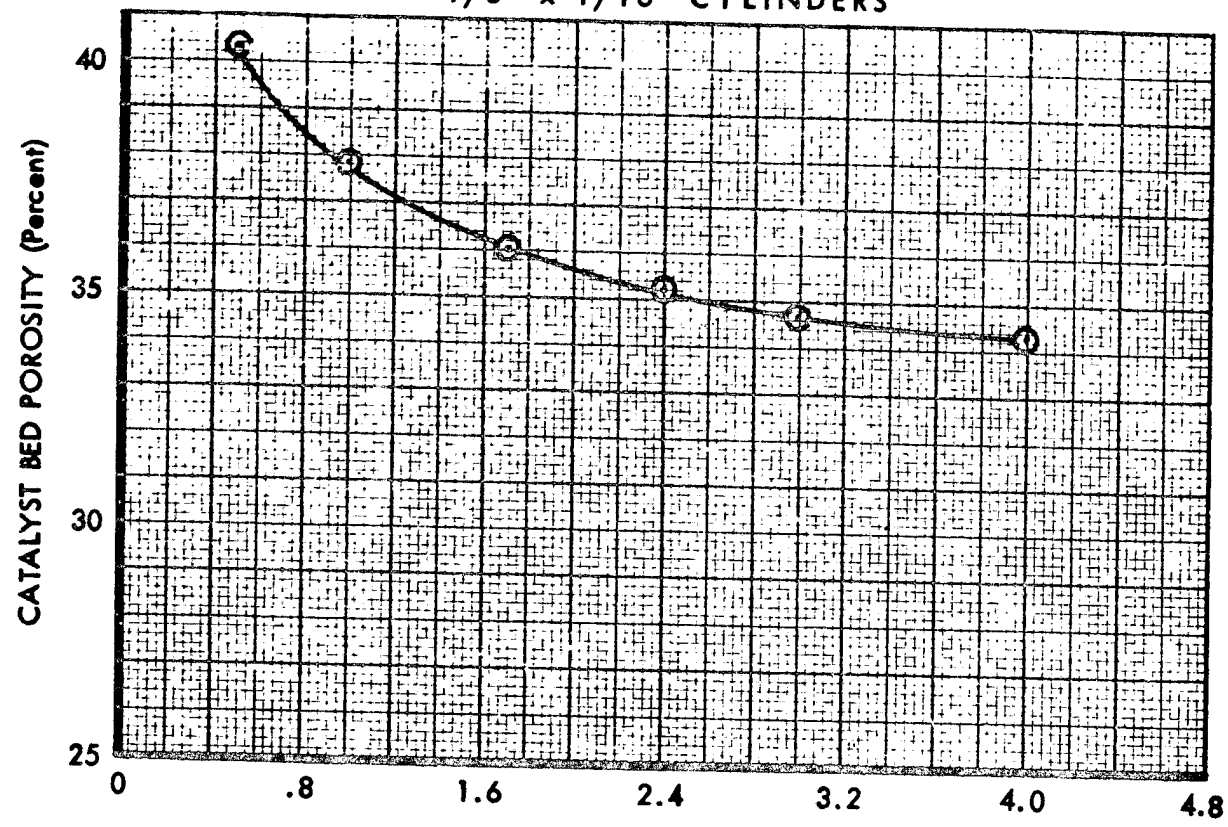

SPECIFIC SURFACE AREA VS CATALYST BED DIAMETER FOR 1/8" x 1/16" CYLINDERS

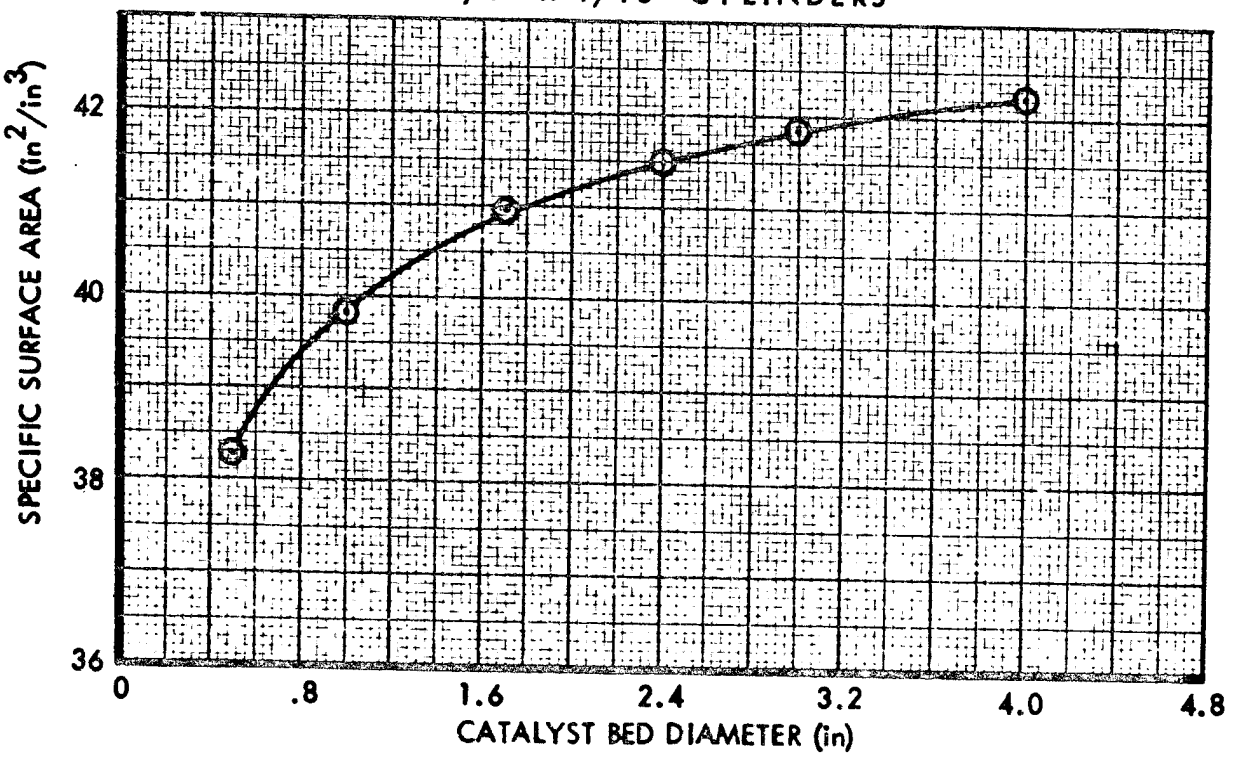

11780

FIGURE 3

CATALYST BED POROSITY
VS
CATALYST BED DIAMETER
FOR
5-8 MESH GRANULAR PARTICLES

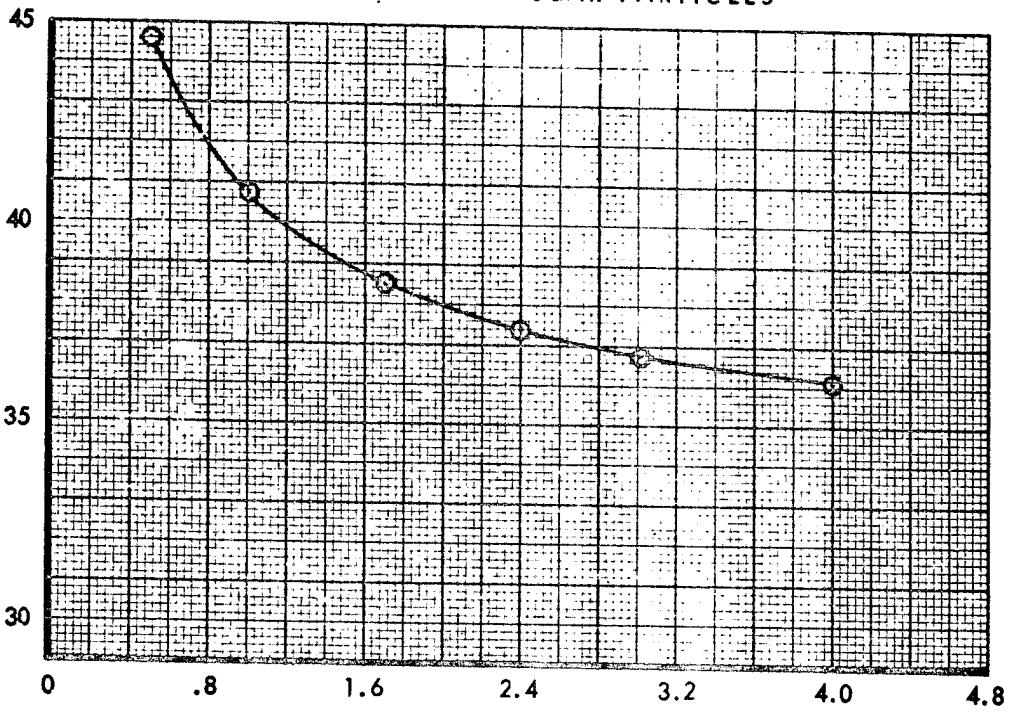

SPECIFIC SURFACE AREA
VS
CATALYST BED DIAMETER
FOR
5-8 MESH GRANULAR PARTICLES

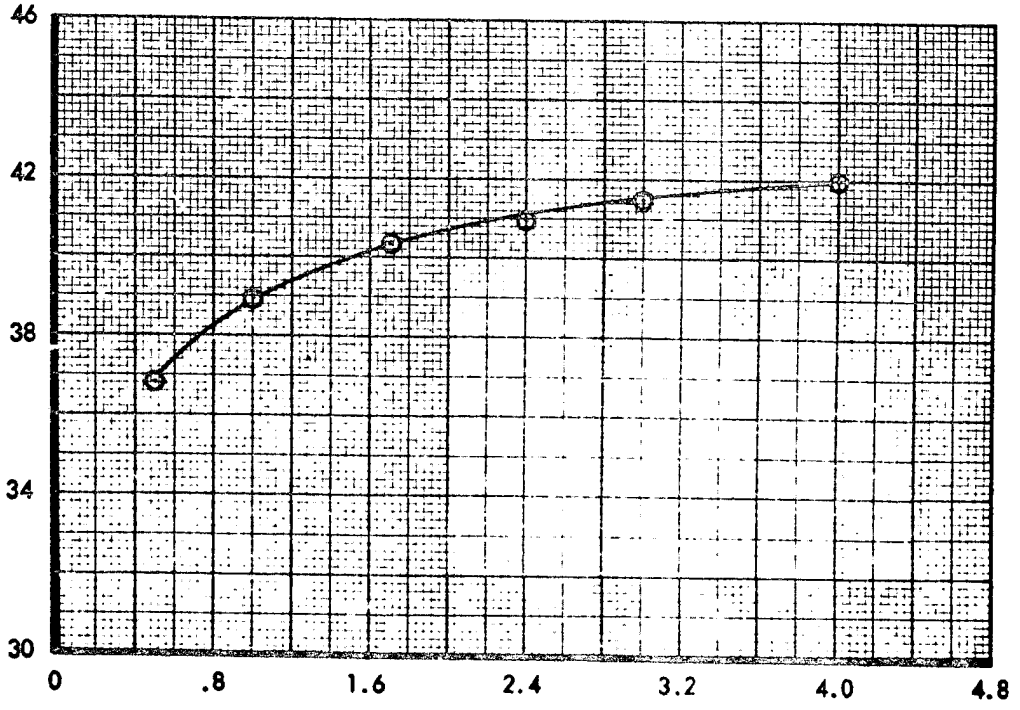

11781

FIGURE

CATALYST BED POROSITY VS CATALYST BED DIAMETER FOR 10-20 MESH GRANULAR PARTICLES

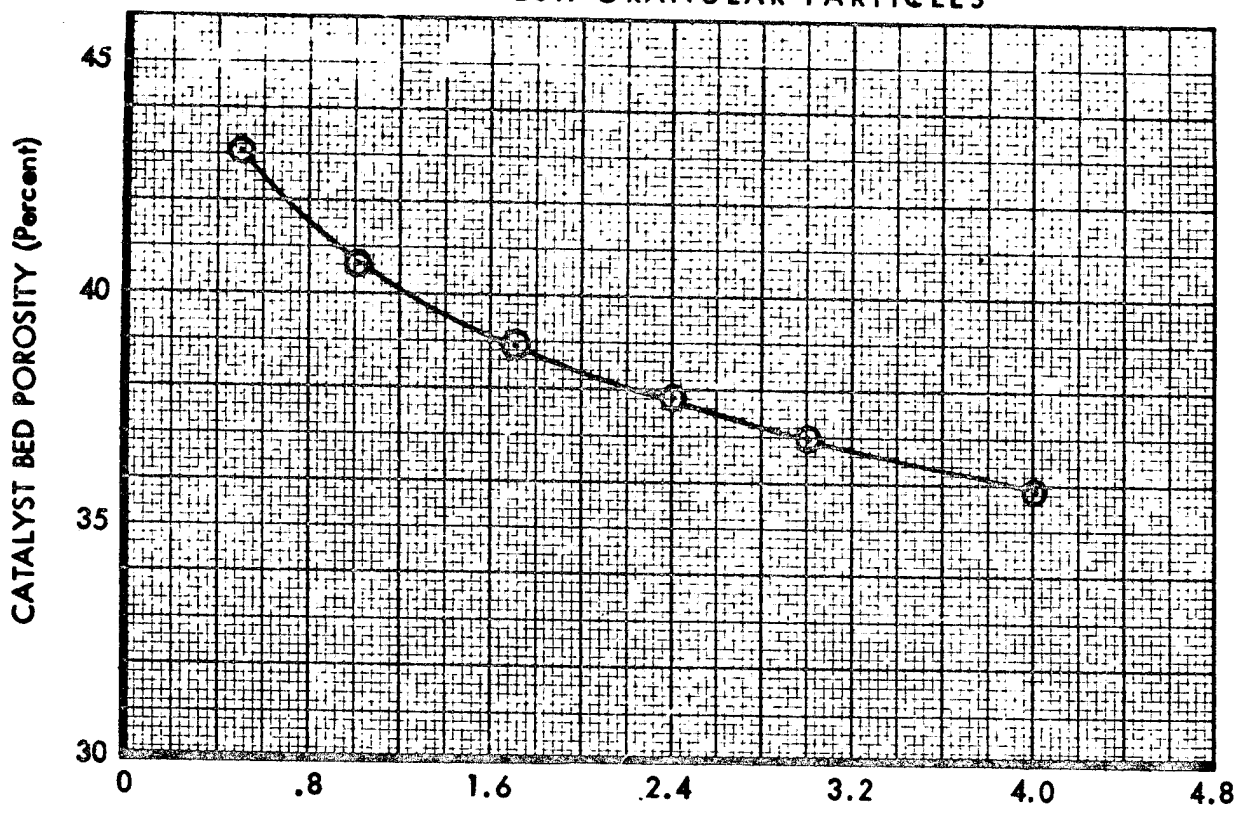

SPECIFIC SURFACE AREA VS CATALYST BED DIAMETER FOR 10-20 MESH GRANULAR PARTICLES

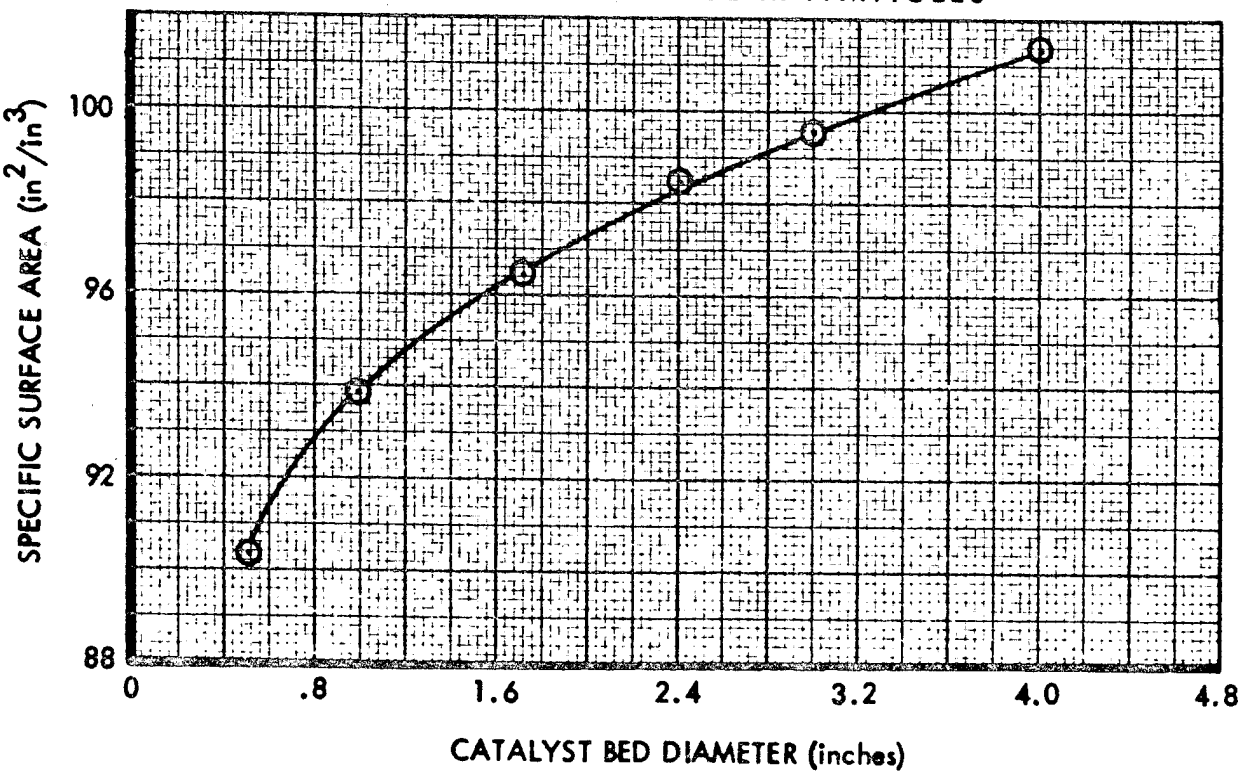

11782

FIGURE 5

CATALYST BED POROSITY
VS CATALYST BED DIAMETER
FOR 20-30 MESH GRANULAR PARTICLES

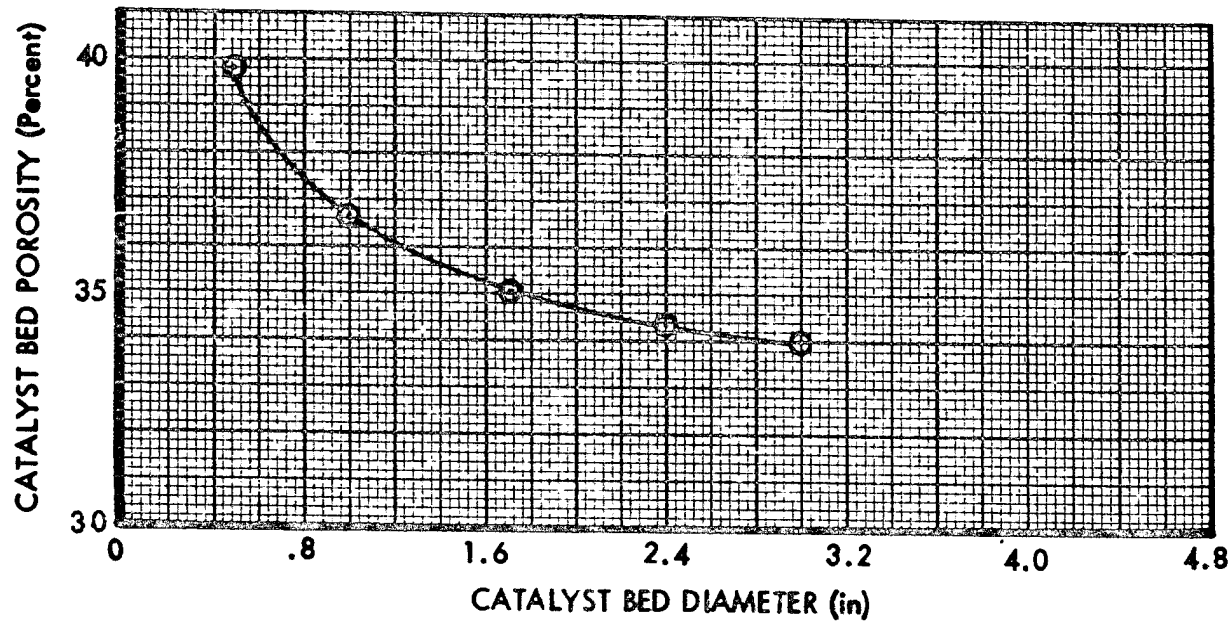

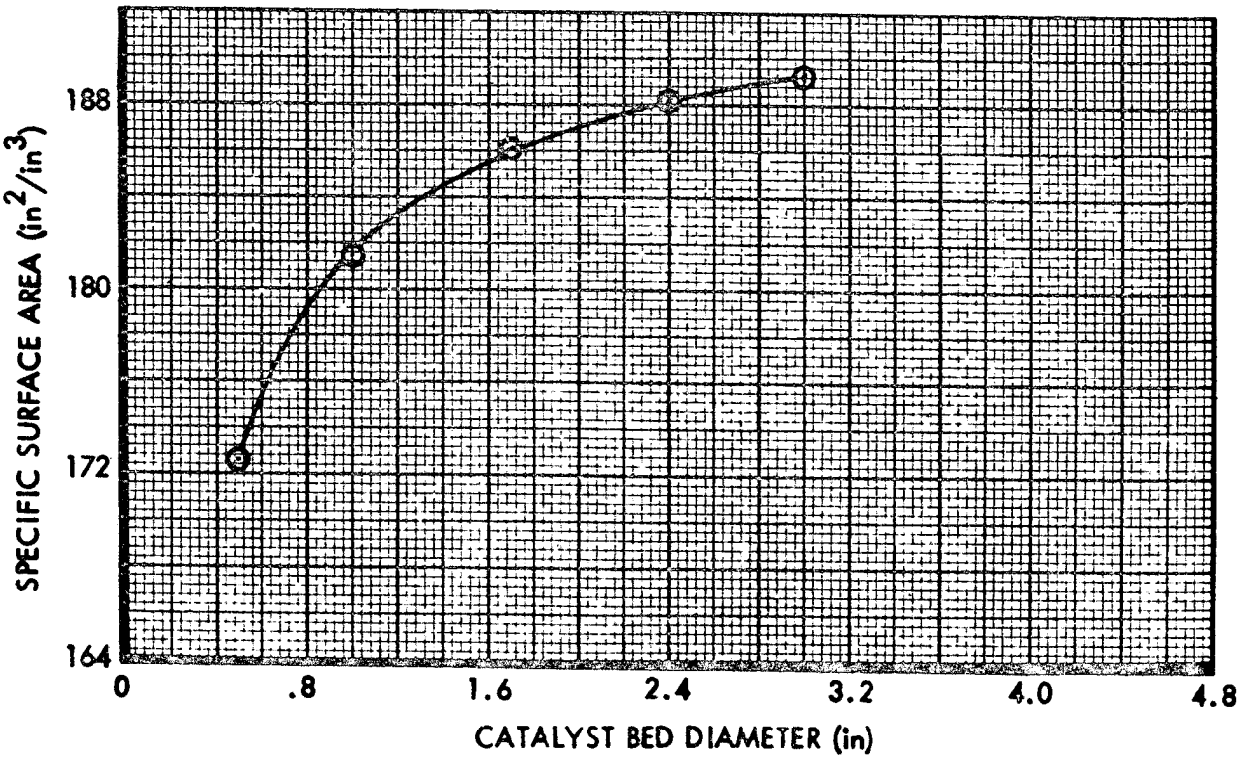

11783

FIGURE 6

EFFECT OF BED LOADING ON AMMONIA DISSOCIATION FOR 50 lbf ENGINE

CHAMBER PRESSURE = 225 psia

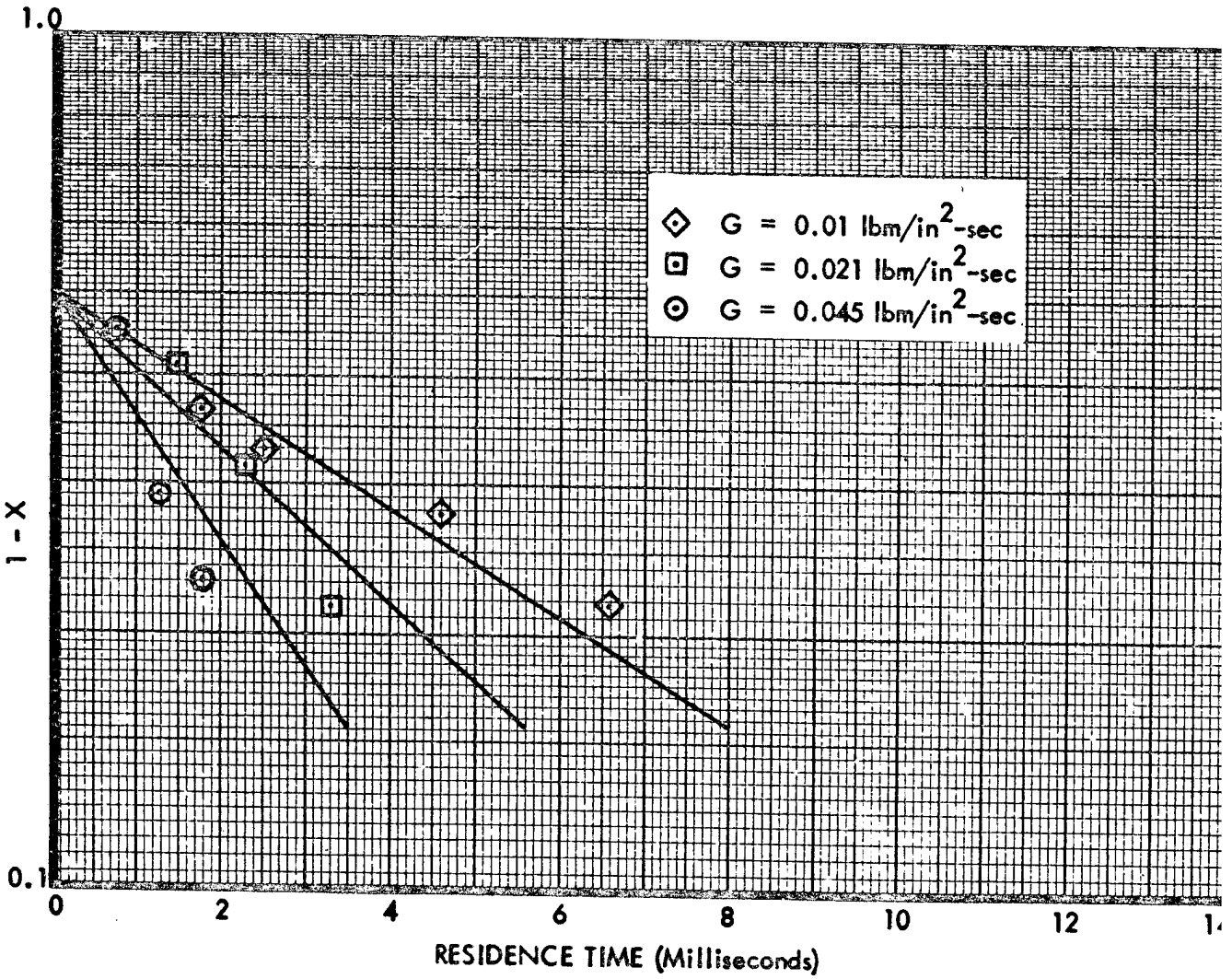

EFFECT OF BED LOADING ON AMMONIA DISSOCIATION FOR 5 lbf ENGINE

CHAMBER PRESSURE = 225 psia

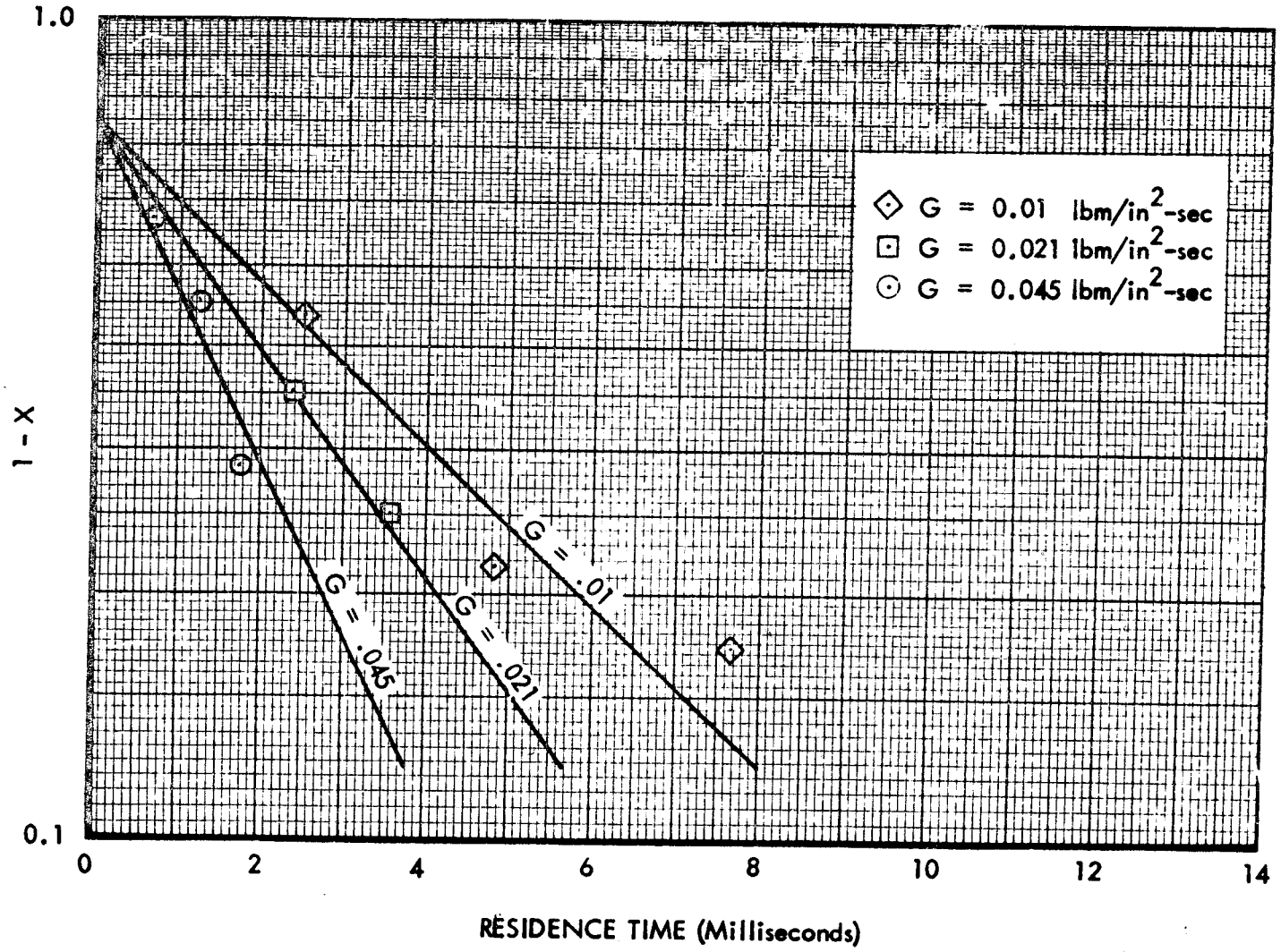

FIGURE 8

EFFECT OF BED LOADING

ON AMMONIA DISSOCIATION

FOR 0.5 lbf ENGINE CHAMBER PRESSURE = 225 psia

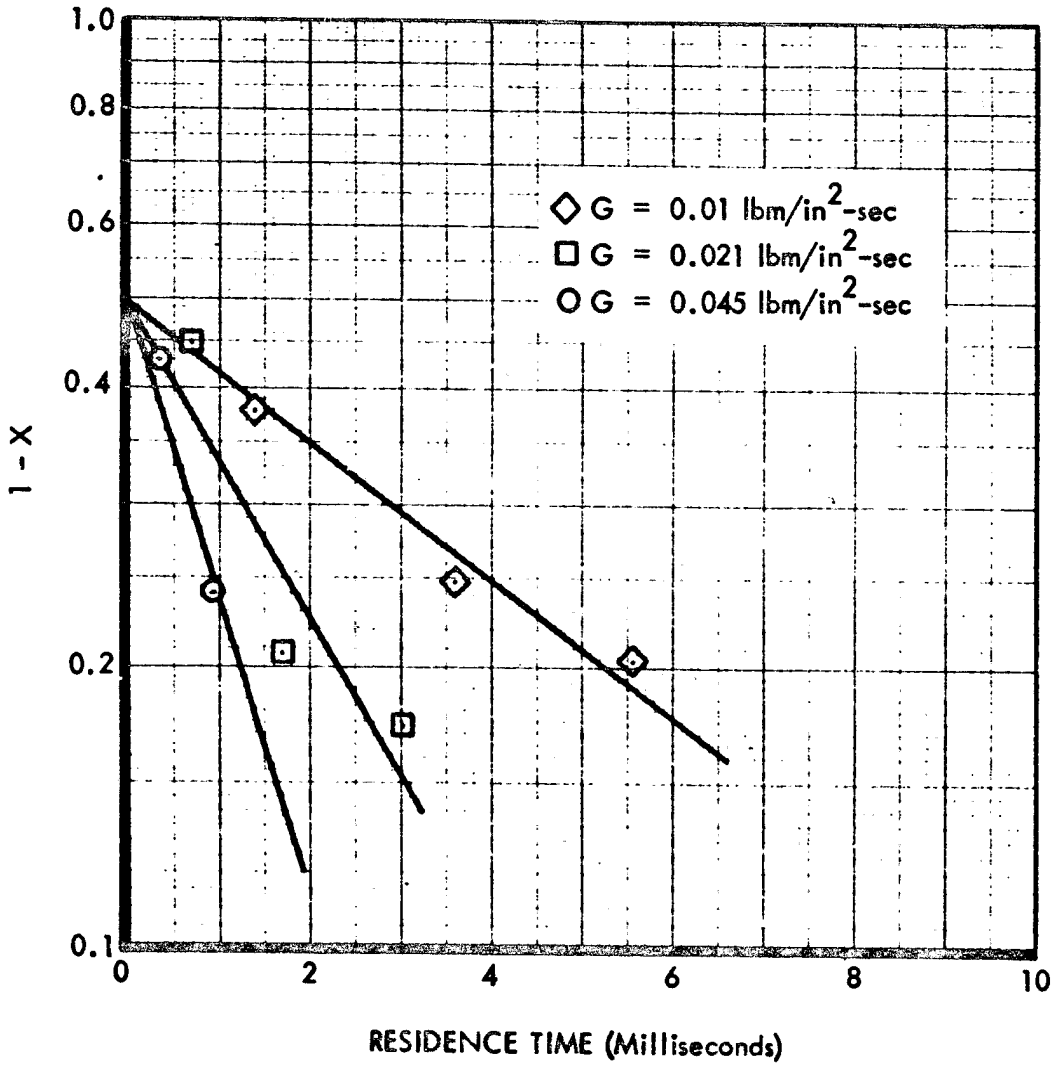

AMMONIA DISSOCIATION MODEL SCHEMATIC

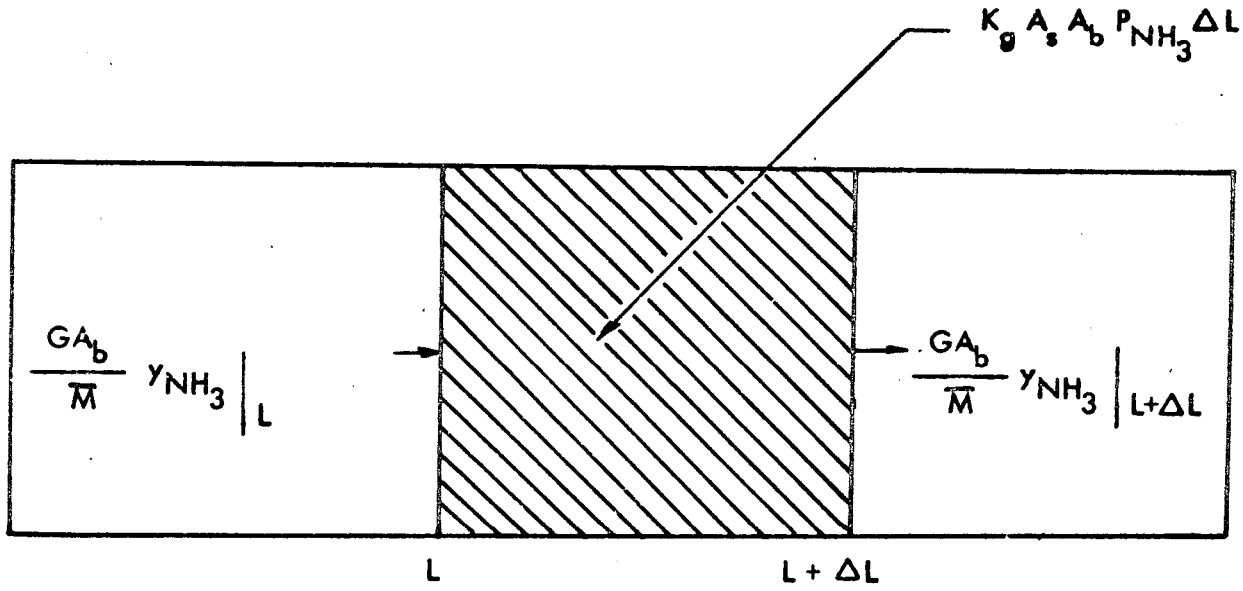

FIGURE 10

RATIO OF RESIDENCE TIME TO CHAMBER PRESSURE
VS
BED LOADING FOR 5 lbf ENGINE

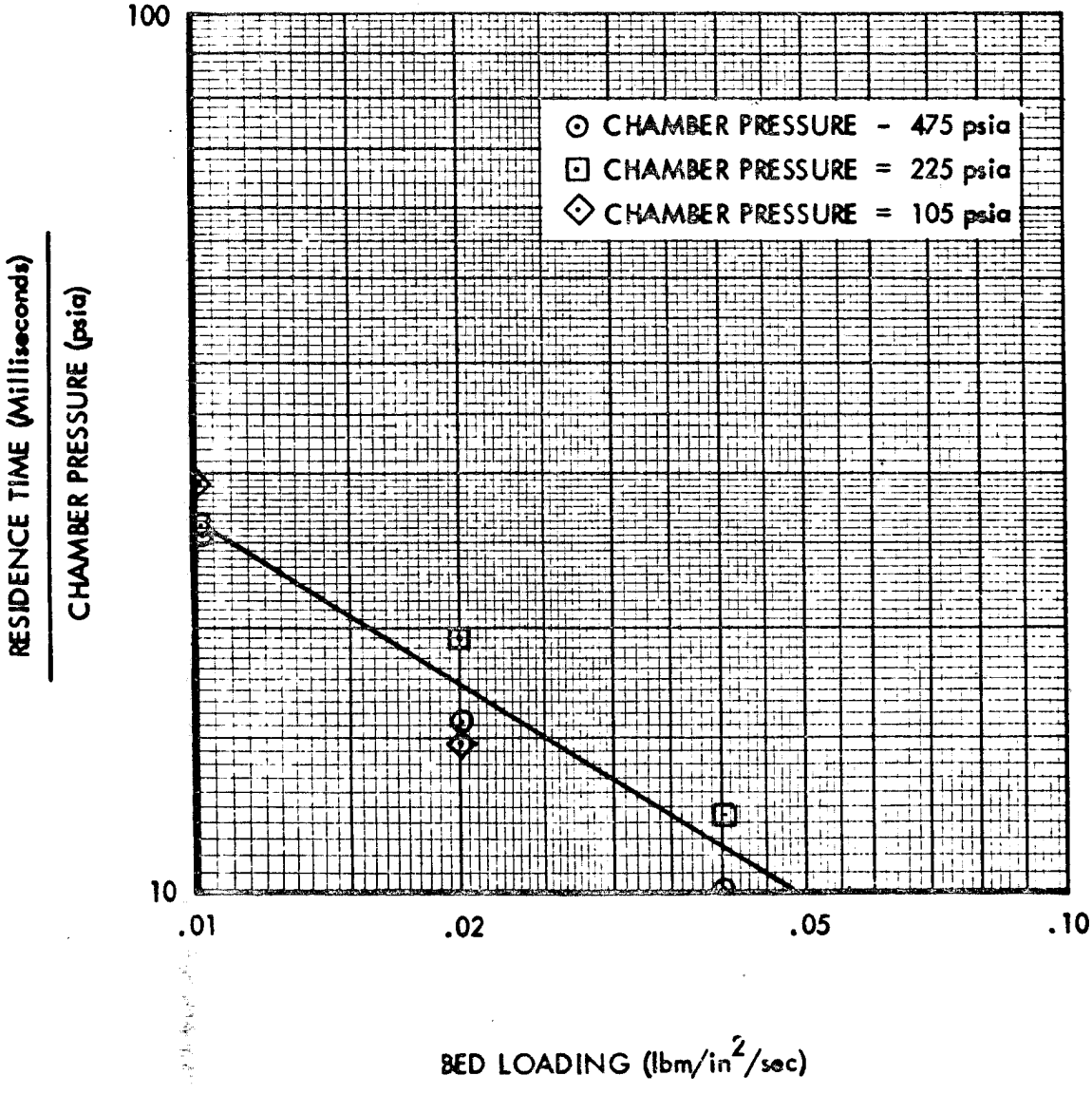

11787

FIGURE 11

RATIO OF RESIDENCE TIME
TO CHAMBER PRESSURE
VS BED LOADING
FOR 50 lbf ENGINE

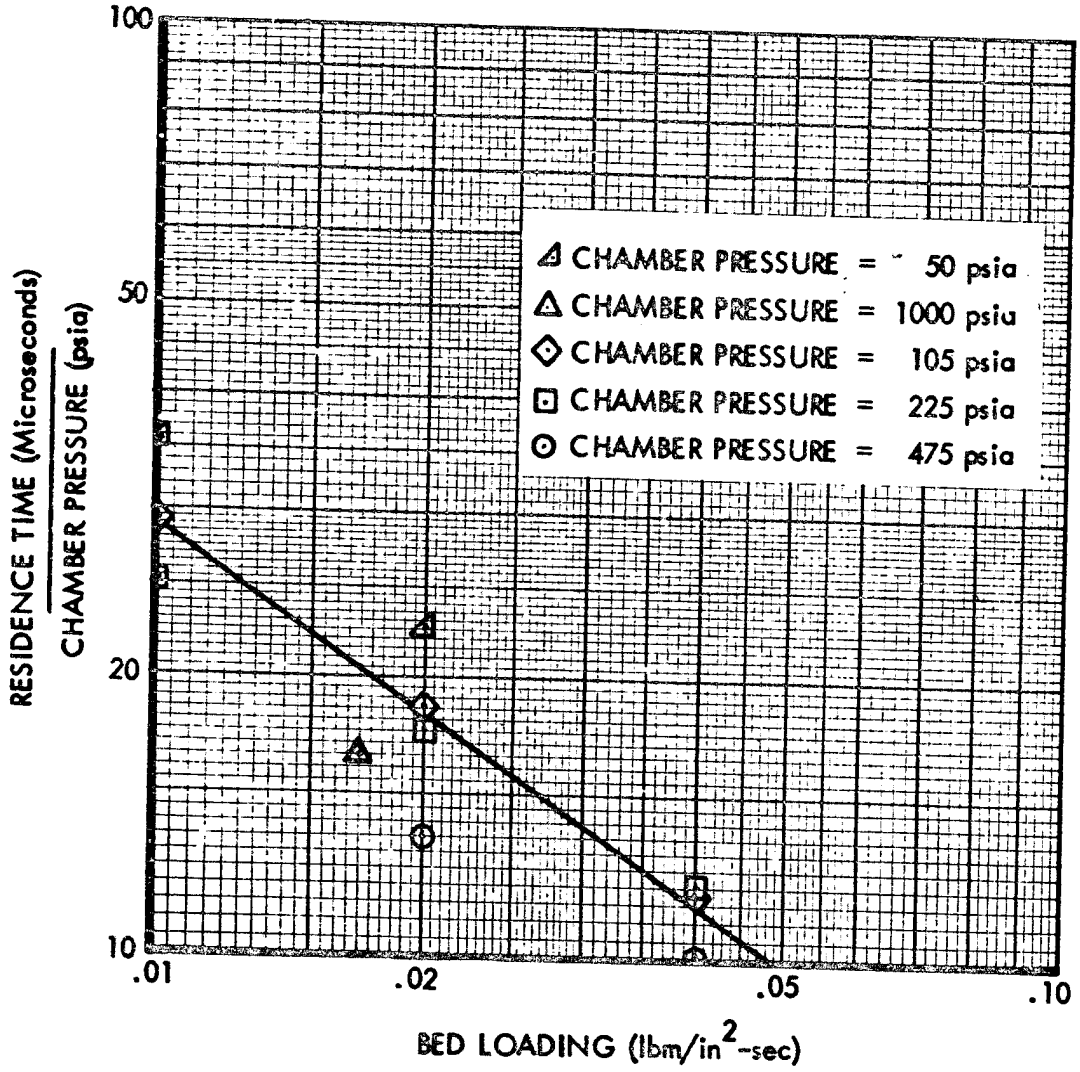

11788

FIGURE 12

RATIO OF RESIDENCE TIME

TO CHAMBER PRESSURE

VS BED LOADING FOR 0.5 lbf ENGINE

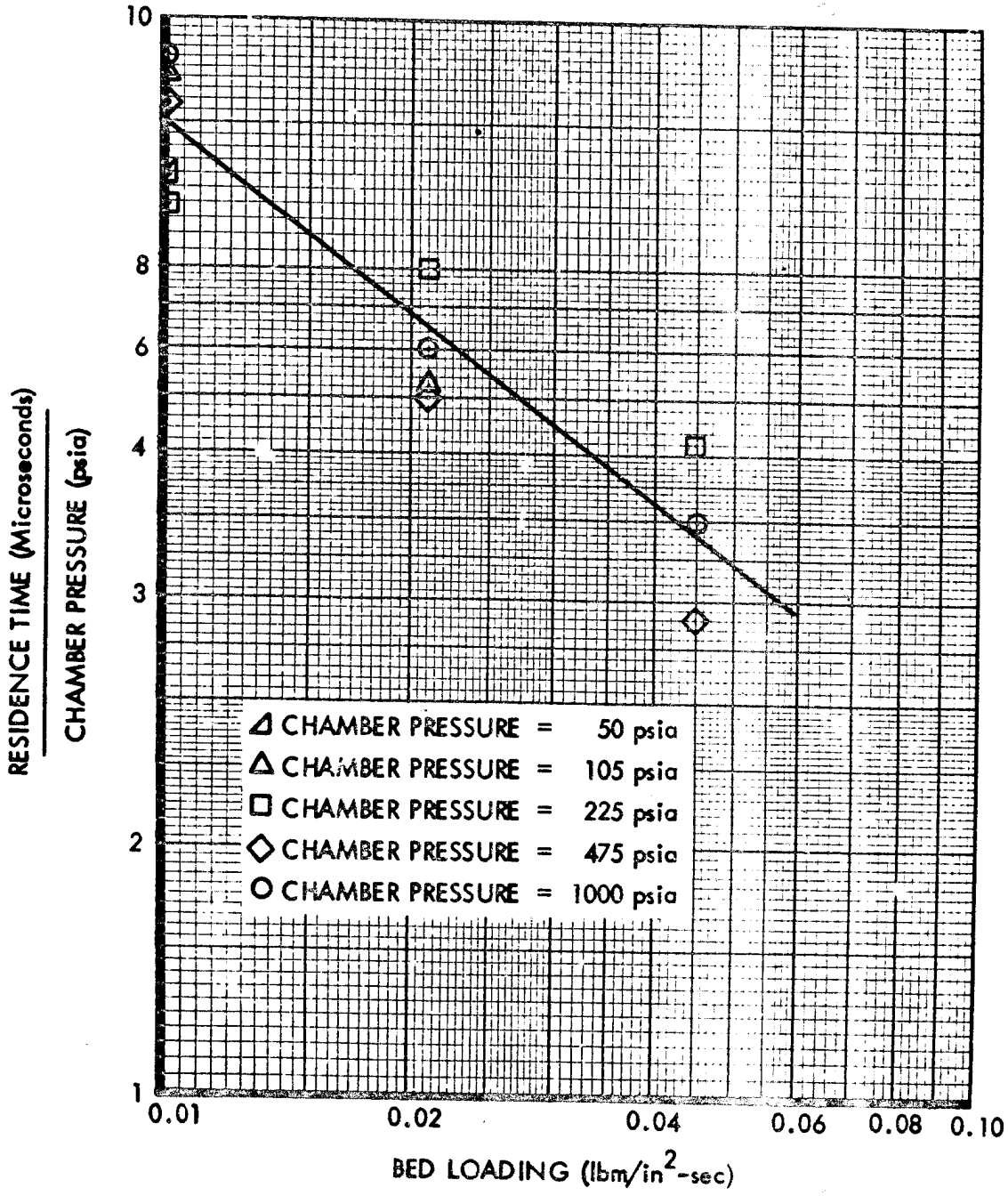

11790

FIGURE 13

EFFECT OF BED LOADING, RESIDENCE TIME, AND CHAMBER PRESSURE
FRACTIONAL AMMONIA DISSOCIATION FOR 5 lbf ENGINE

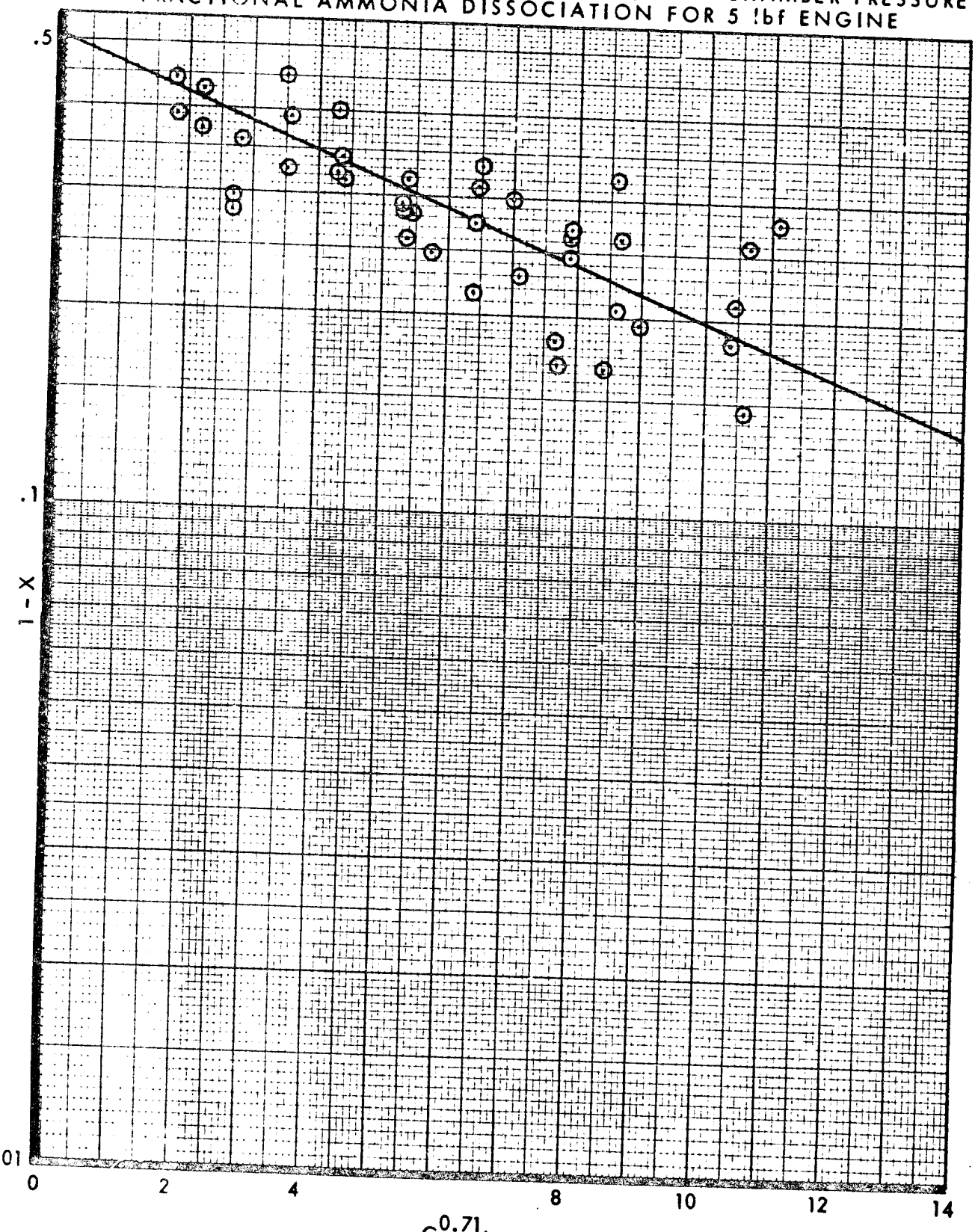

11789

FIGURE 14

EFFECT OF BED LOADING, RESIDENCE TIME,
AND CHAMBER PRESSURE ON FRACTIONAL AMMONIA DISSOCIATION
FOR 50 lbf ENGINE

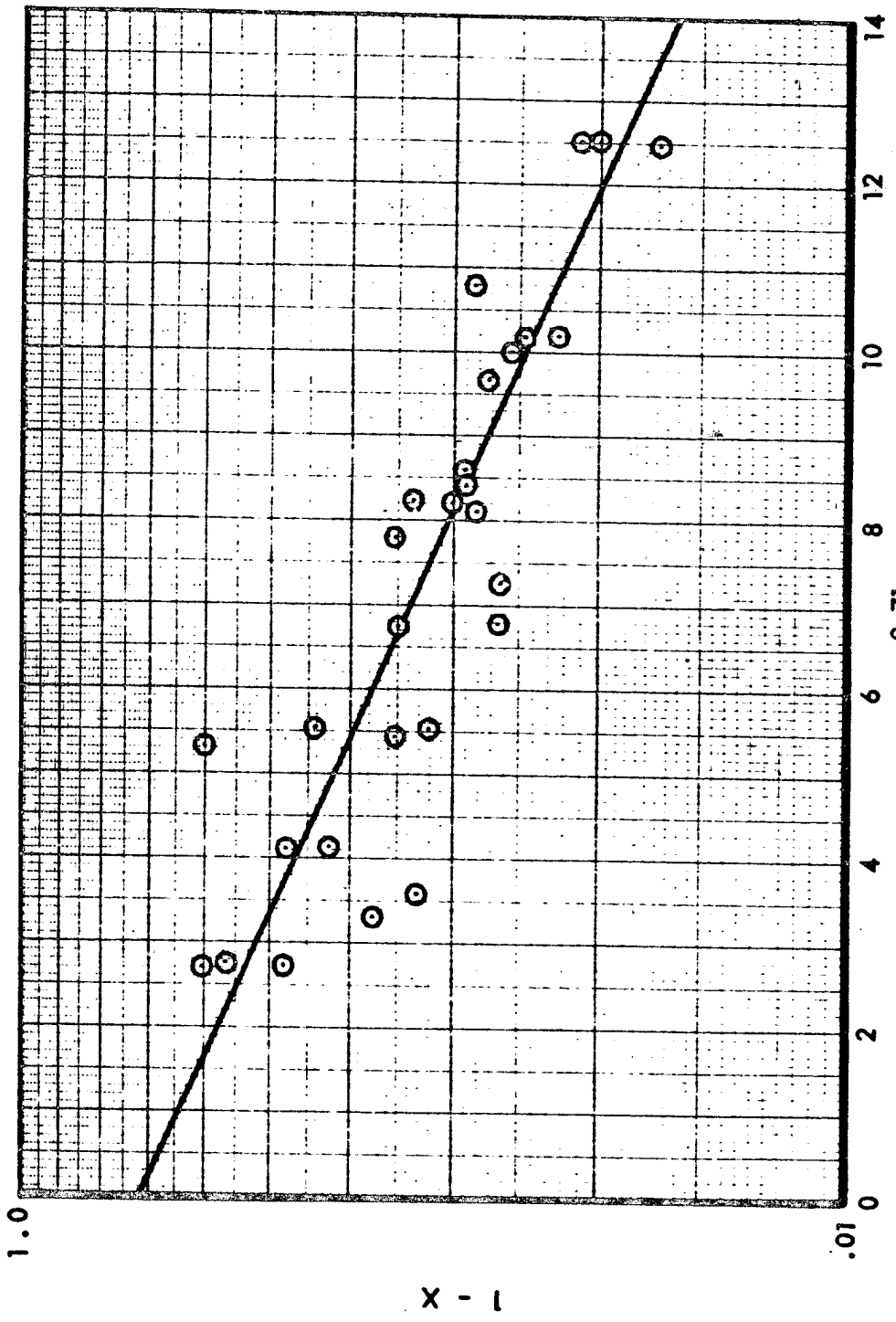

11776

FIGURE 15

CORRELATION OF AMMONIA DISSOCIATION DATA
0.5 lbf ENGINE

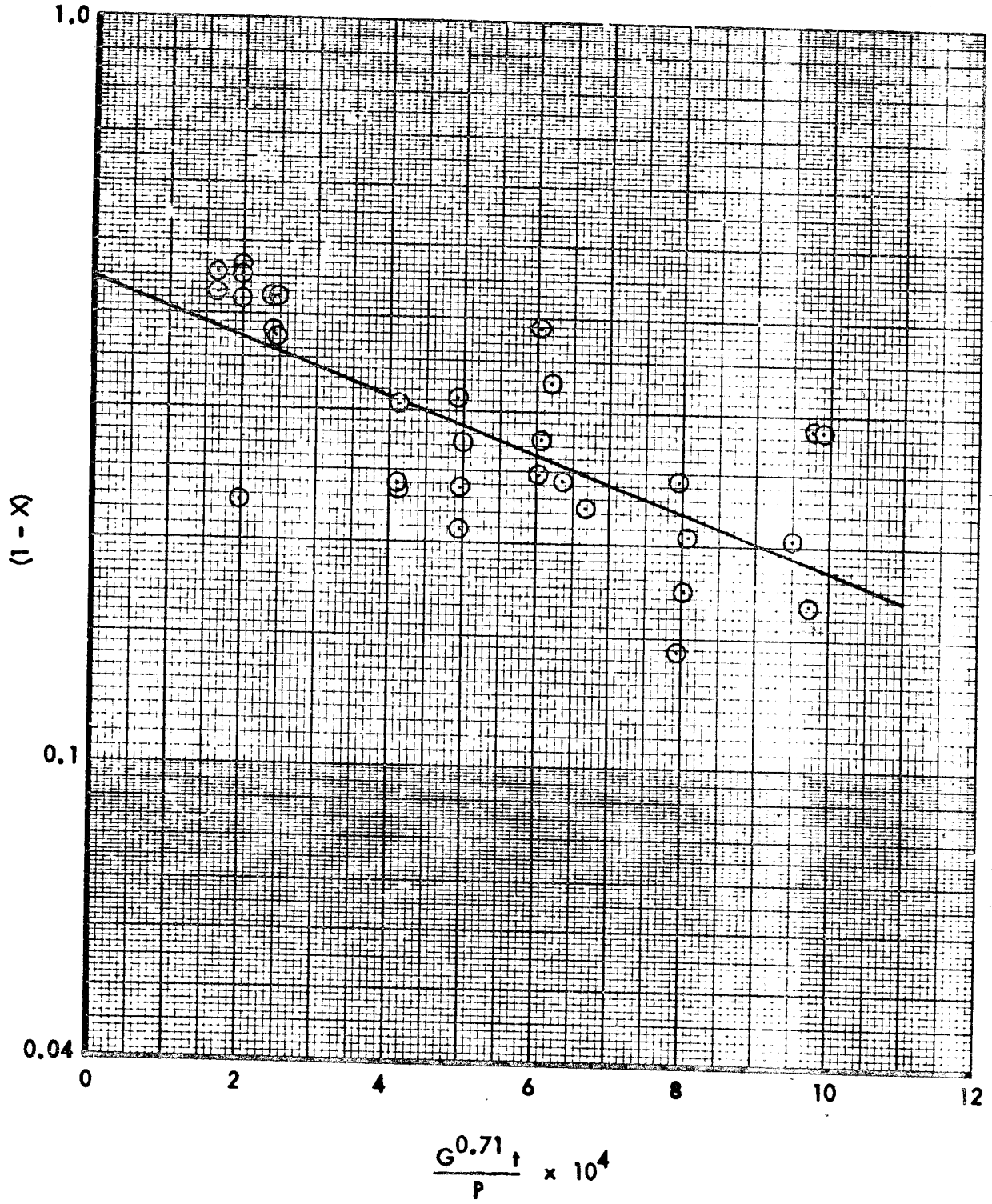

12133

FIGURE 16

GENERAL CORRELATION OF AMMONIA DISSOCIATION DATA

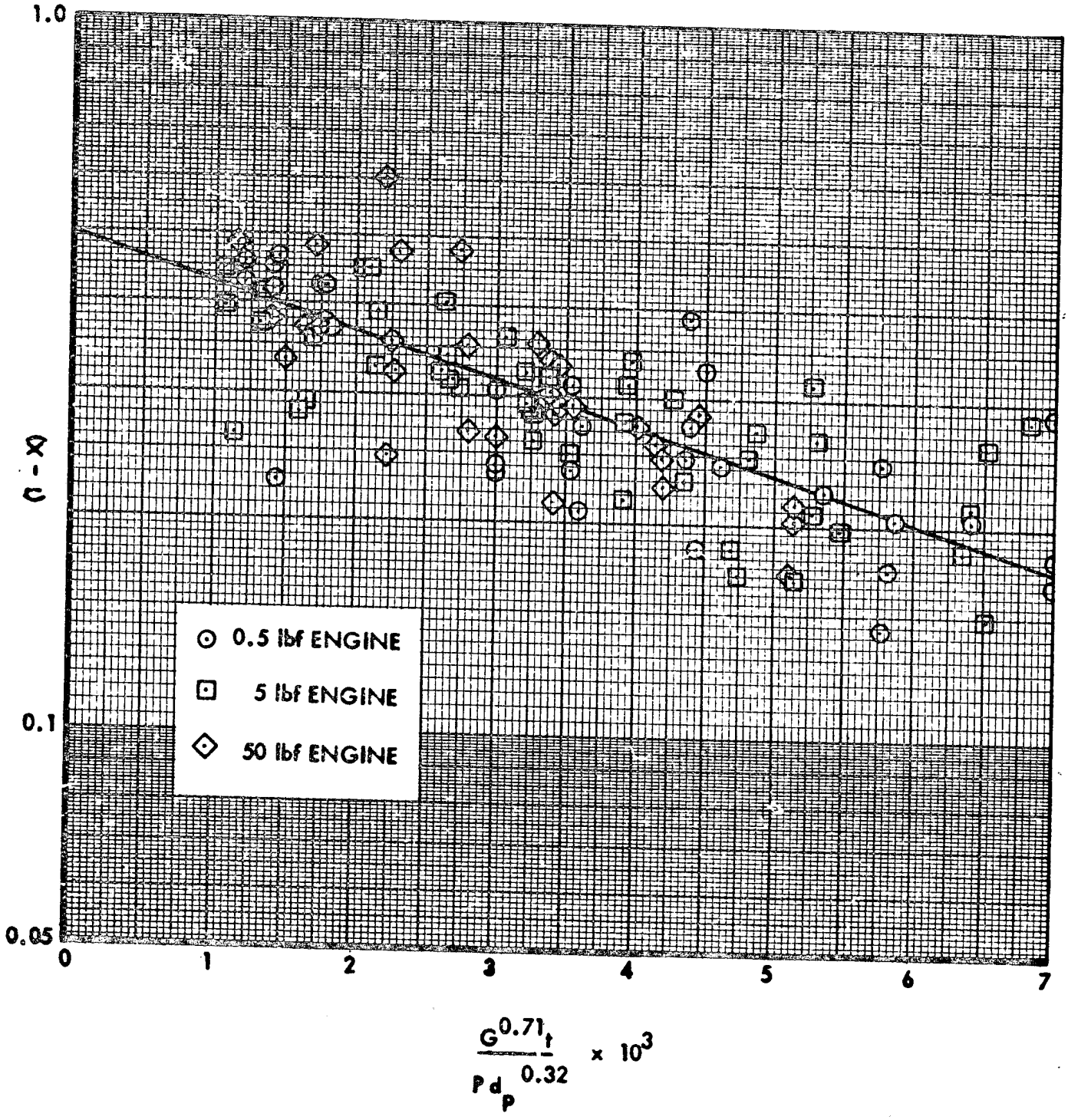

12134

FIGURE 17

EFFECT OF CHAMBER PRESSURE ON
CATALYST BED LENGTH REQUIREMENTS
5 lbf ENGINE

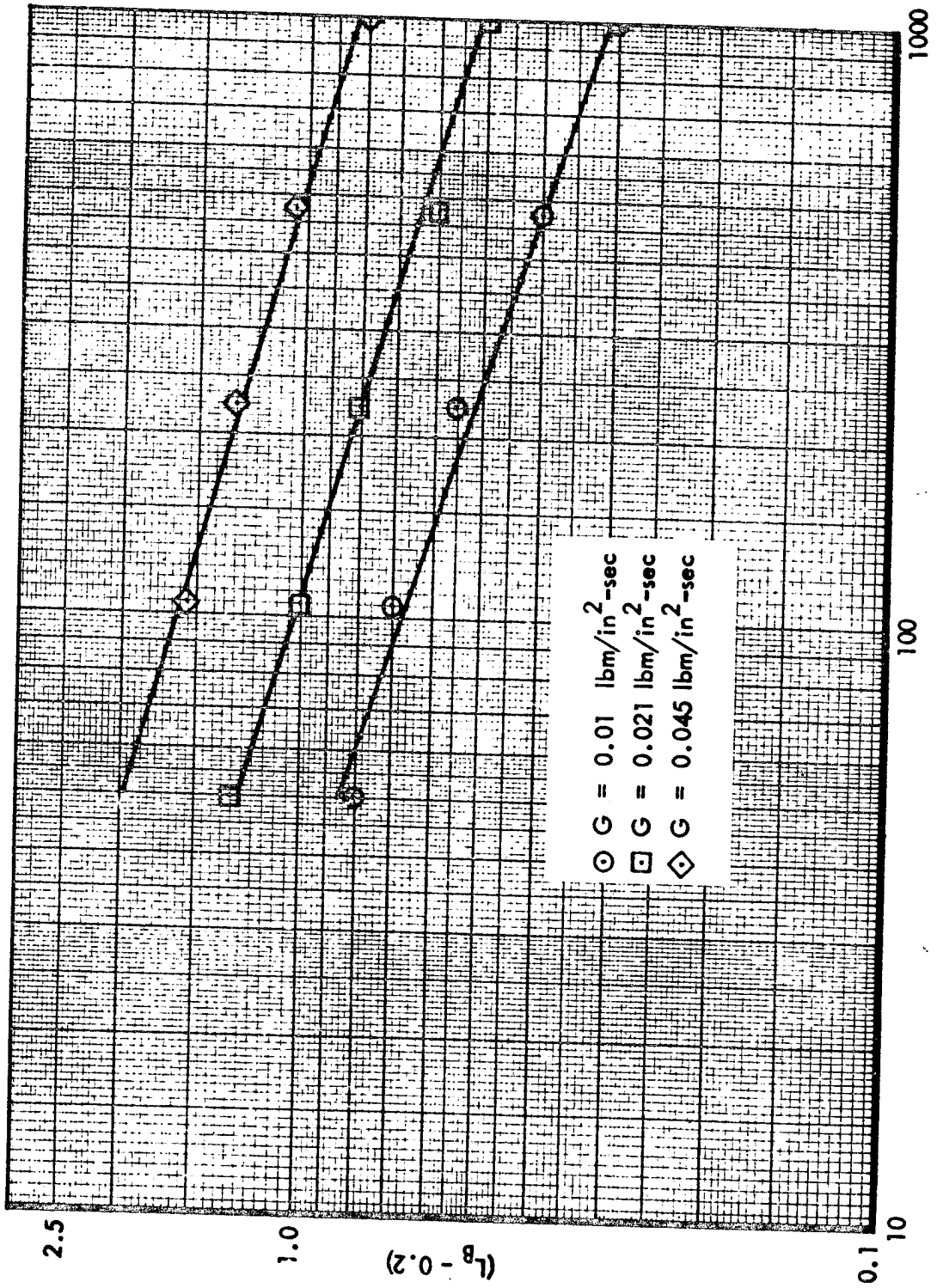

11791

FIGURE 18

EFFECT OF CHAMBER PRESSURE ON CATALYST BED LENGTH REQUIREMENTS 50 lbf ENGINE

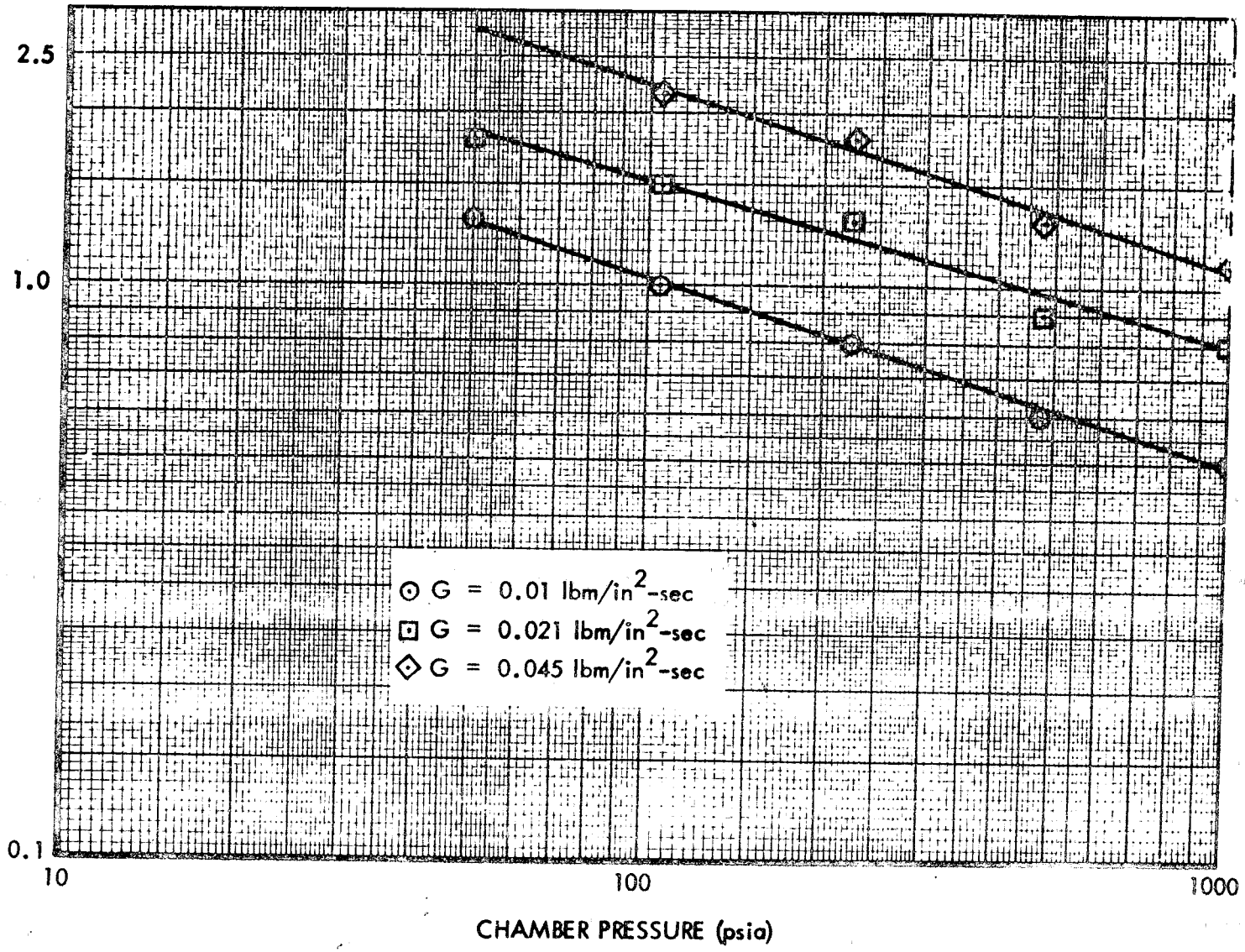

FIGURE 19

EFFECT OF BED LOADING ON
CATALYST BED LENGTH REQUIREMENTS
5 lbf ENGINE

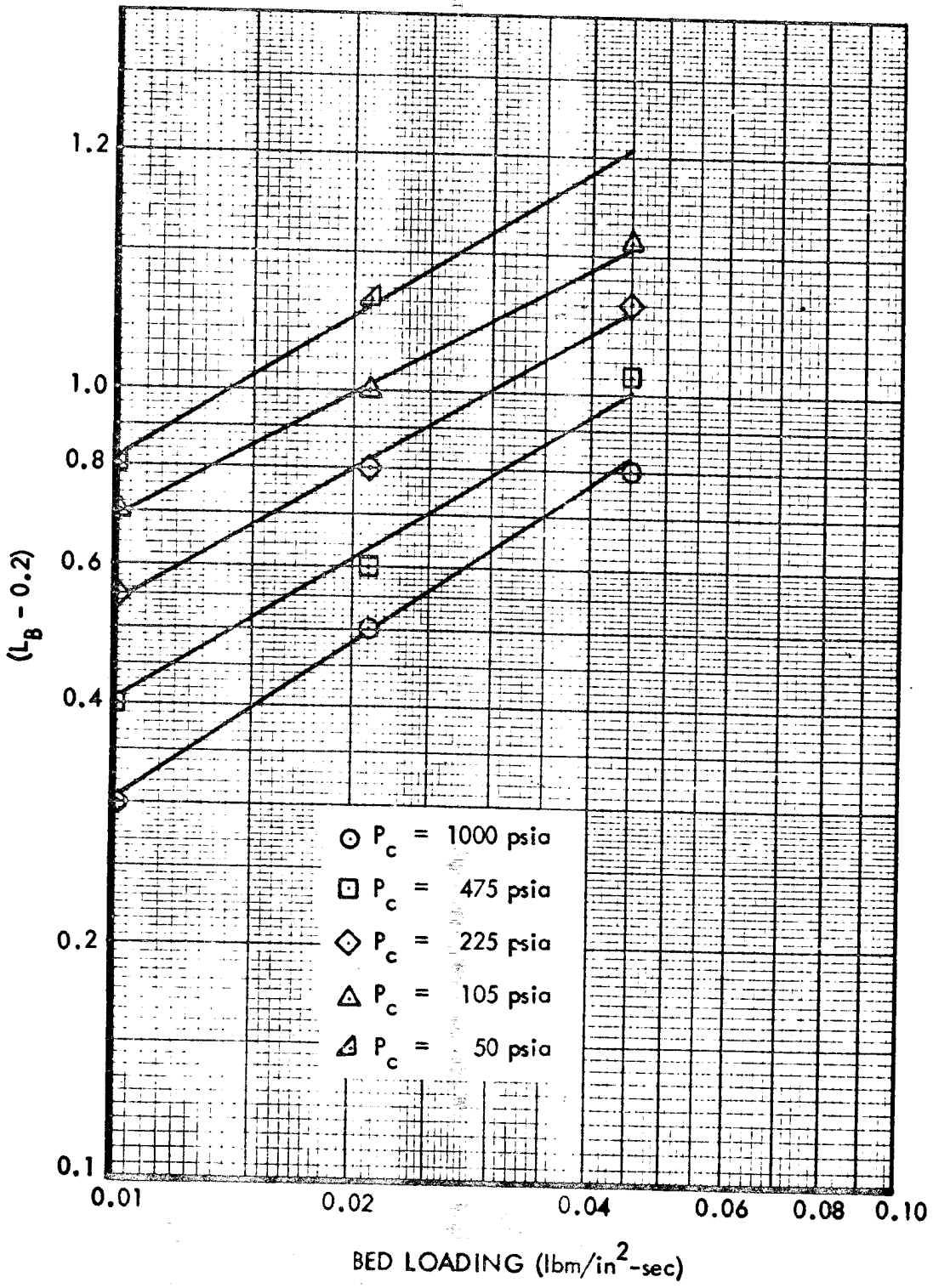

11793

FIGURE 20

EFFECT OF BED LOADING ON
CATALYST BED LENGTH REQUIREMENTS
50 lbf ENGINE

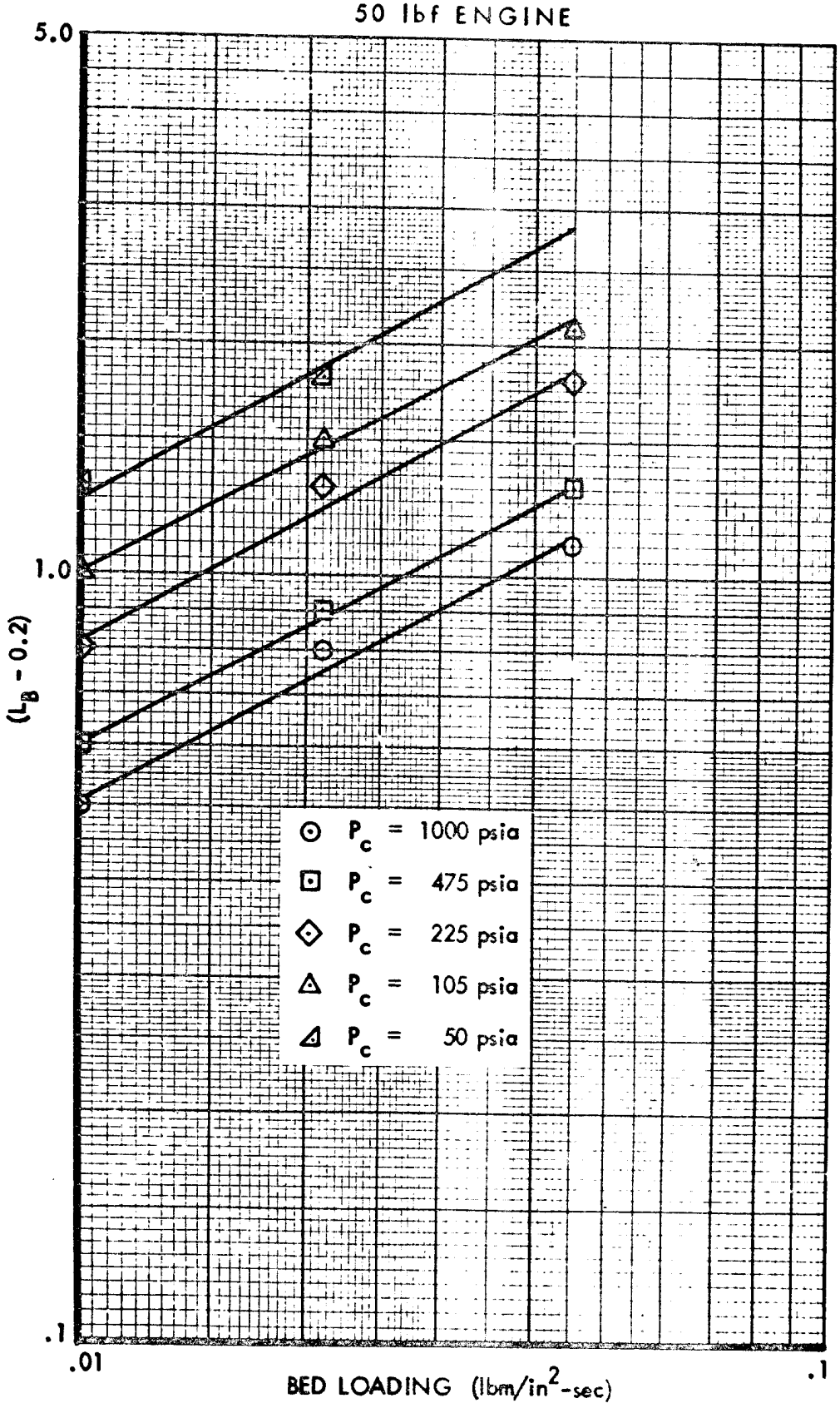

11794

FIGURE 21

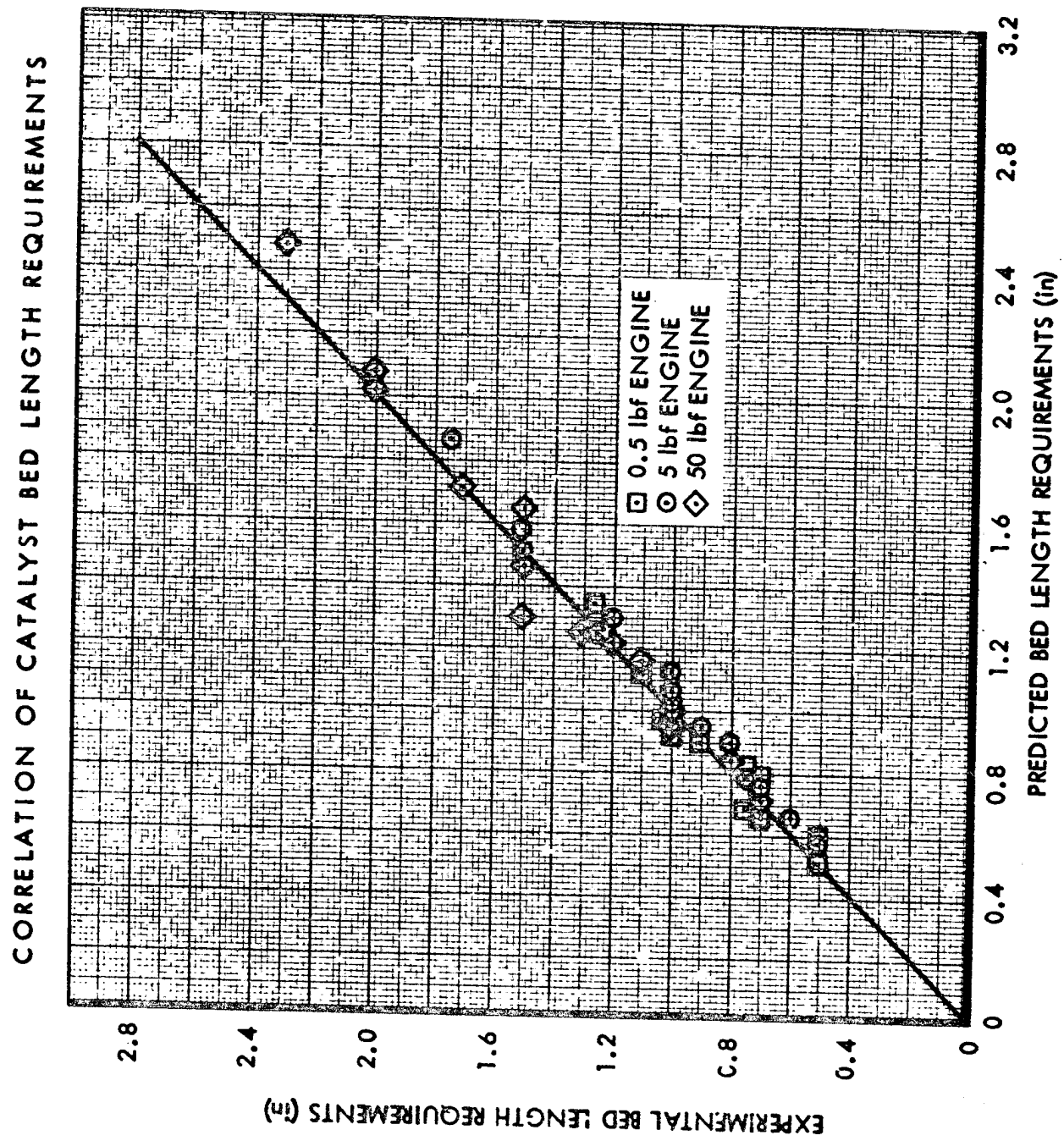

11796

FIGURE 22

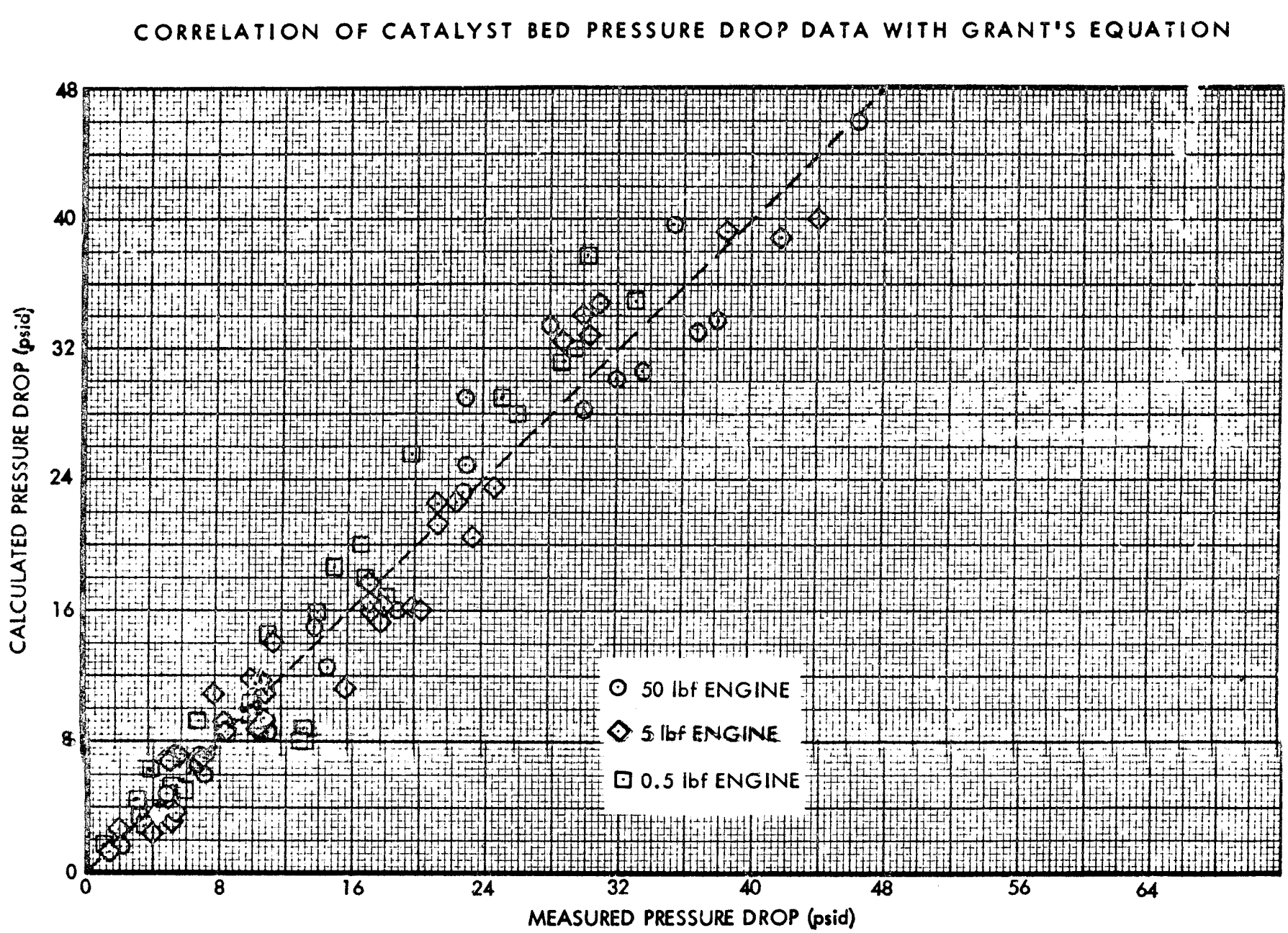
CORRELATION OF CATALYST BED PRESSURE DROP DATA WITH GRANT'S EQUATION
CALCULATED PRESSURE DROP (psid)
MEASURED PRESSURE DROP (psid)
0
8
16
24
32
40
48
56
64
50 lbf ENGINE
5 lbf ENGINE
0.5 lbf ENGINE

FIGURE 23

5 lbf ENGINE CATALYST BED PRESSURE DROP MODIFIED ERGUN EQUATION CORRELATION

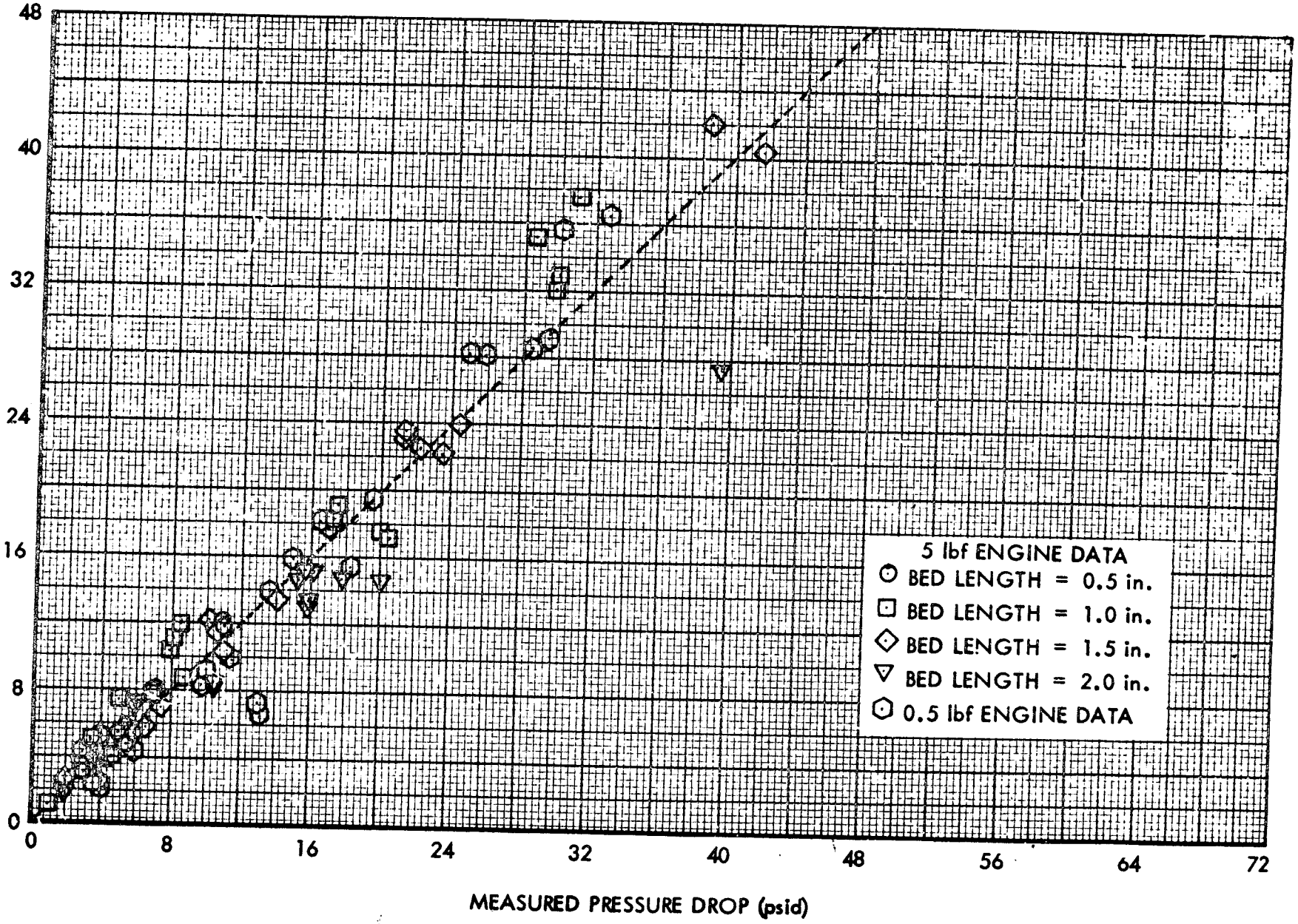

FIGURE 24

PRESSURE RISE MODEL SCHEMATIC STAGE 1

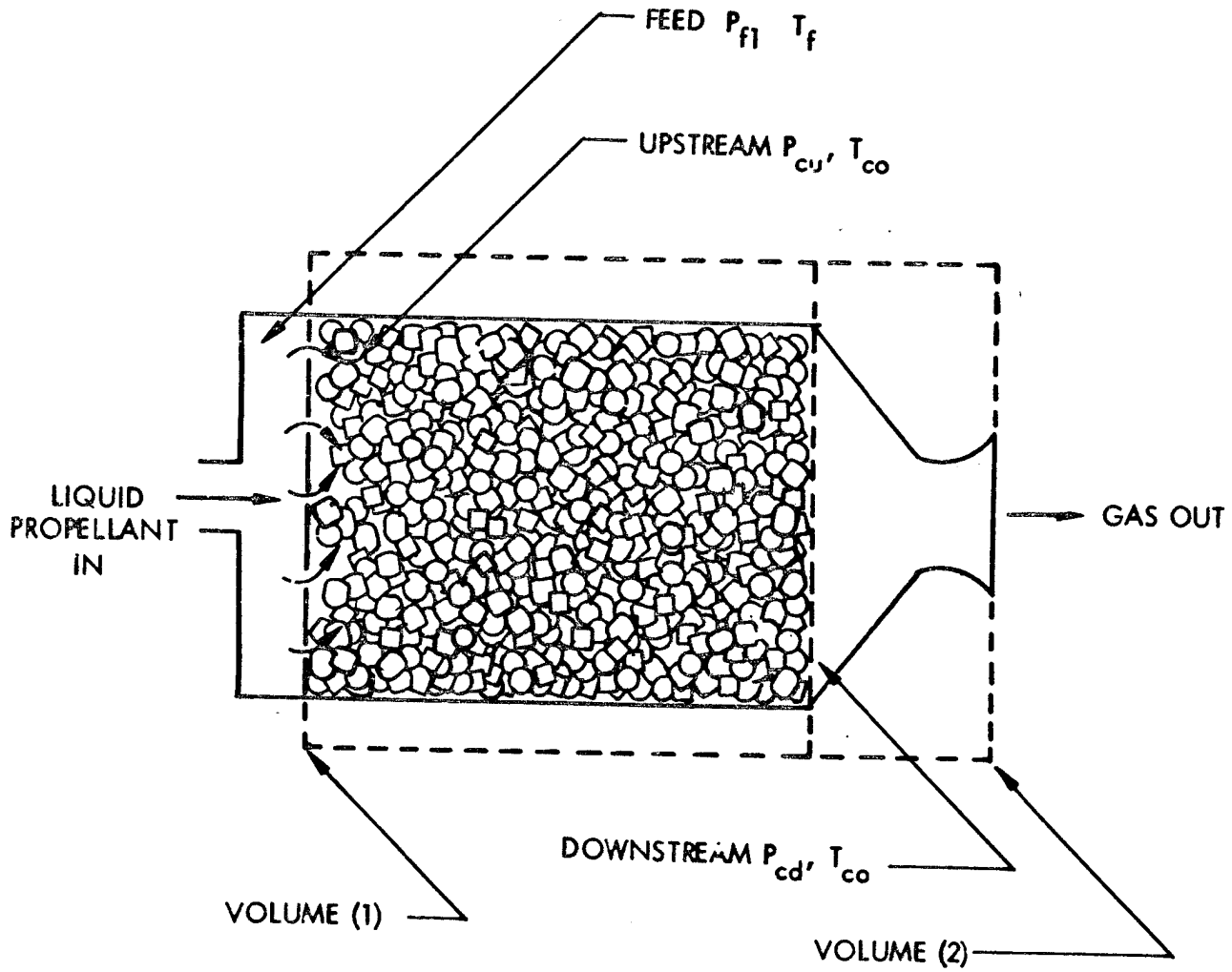

11797

FIGURE 25

PRESSURE RISE MODEL SCHEMATIC
STAGE 2

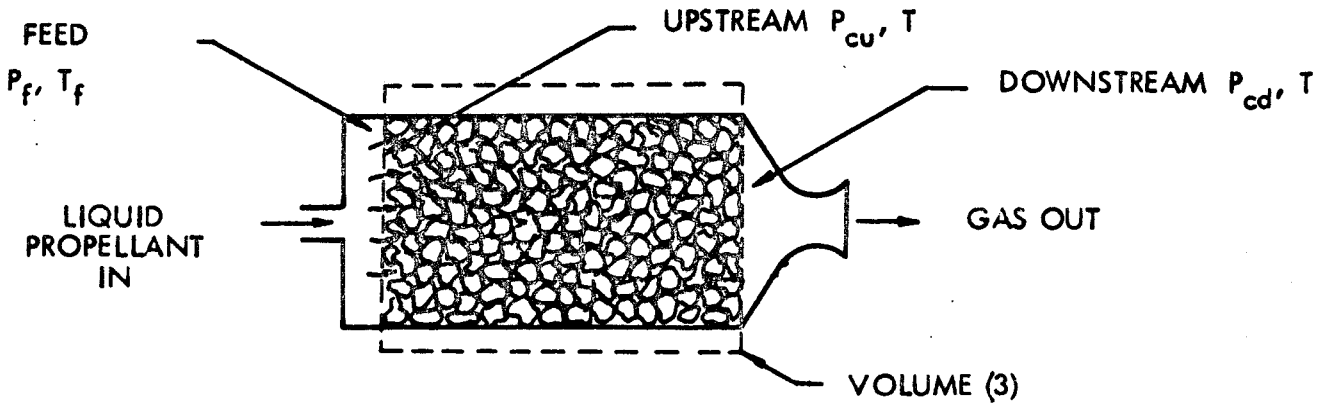

FIGURE 26

STAGE 1 PRESSURE RISE INTEGRAL EVALUATION

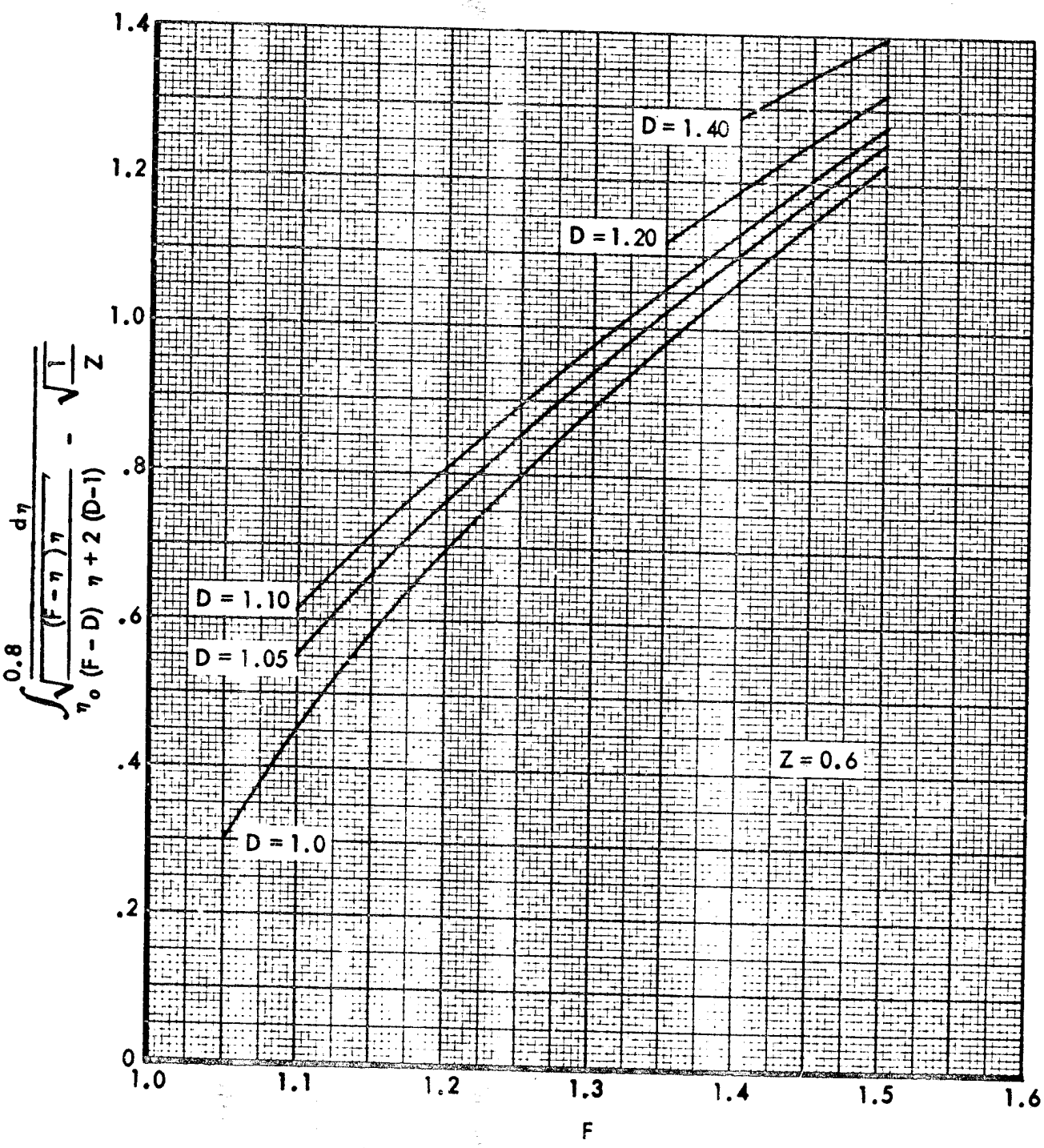

FIGURE 27

EVALUATION OF STAGE 1 PRESSURE RISE CONSTANT

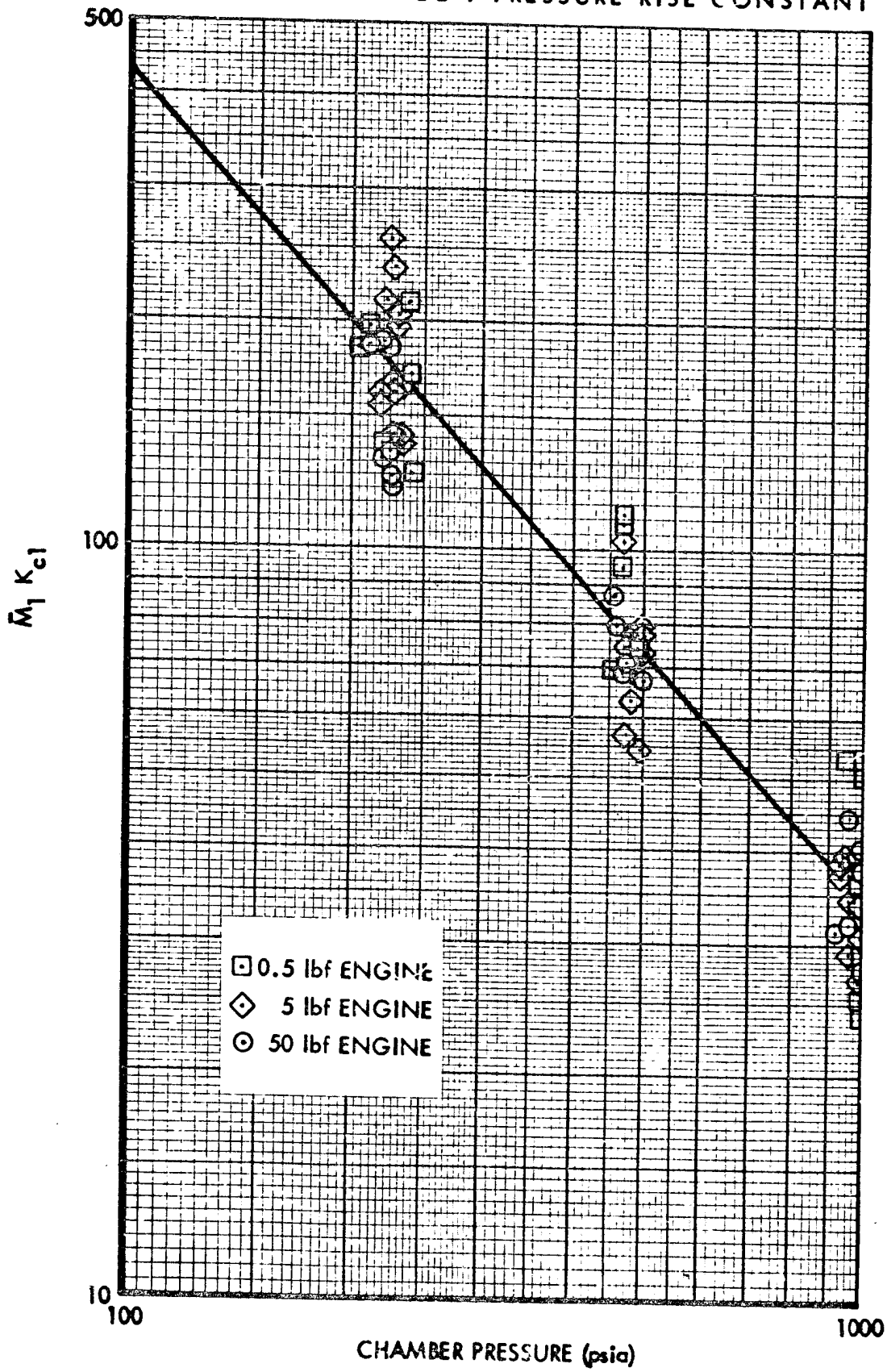

12130

FIGURE 28

12132

FIGURE 29

EVALUATION OF STAGE 2 PRESSURE RISE CONSTANT

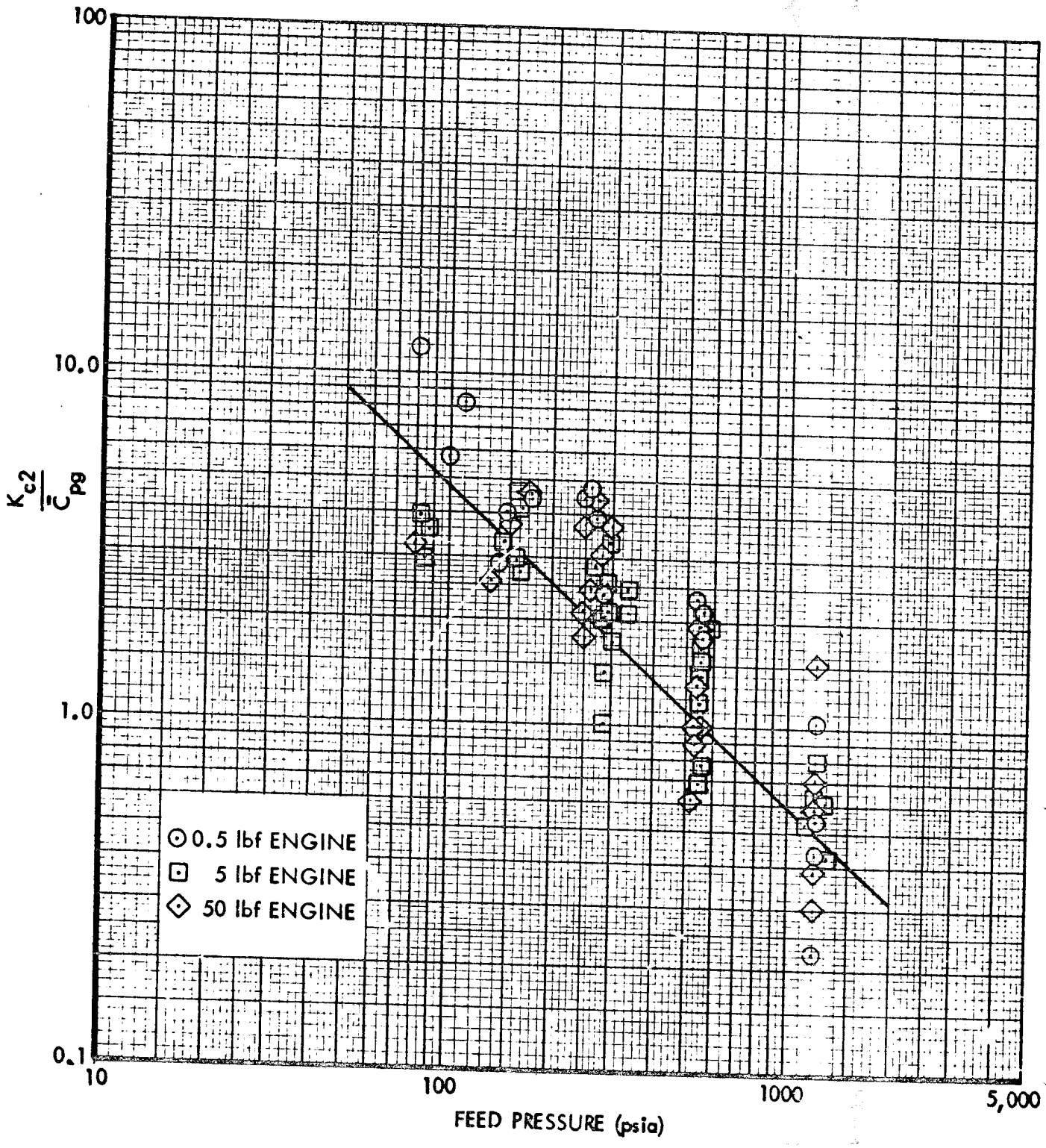

12129

FIGURE 30

APPENDIX I

The following paragraphs illustrate use of the design equations for the 100 lbf engine tested during the program. The following requirements were set for the rocket engine:

Vacuum Thrust = 100 lbf

Chamber Pressure = 200 psia

A delivered vacuum specific impulse of 233 lbf-sec/lbm is assumed. Thus, the engine flow rate is calculated as:

$$\dot{w} = \frac{100}{233} = 0.428 \text{ lbm/sec}$$

A bed loading of 0.045 is chosen as a starting point for the design iteration. Using this bed loading, the chamber diameter is calculated as:

$$D_b = \sqrt{\frac{4}{\pi}\left(\frac{0.428}{0.045}\right)} = 3.48 \text{ inches}$$

For this bed diameter, an 0.2 inch layer of 25-30 mesh catalyst is used at the top of the catalyst bed with the remainder of the bed 1/8" x 1/8" cylindrical pellets.

Using the curves in Section 3.0, the catalyst bed porosity and specific surface area is estimated as:

$A_s = 205 \text{ in}^2/\text{in}^3$	25-30 mesh
$A_s = 32 \text{ in}^2/\text{in}^3$	1/8" x 1/8" pellets
$\epsilon = 0.336$	25-30 mesh
$\epsilon = 0.336$	1/8" x 1/8" pellets

The required catalyst bed length is then calculated as:

$$L_B = 0.2 + 145 \frac{(0.045)^{0.554}}{(200)^{0.3}\,(32)^{0.3}}$$

$$L_B = 0.2 + 1.87 = 2.07 \text{ inches}$$

The Reynolds Number for flow through each of the catalyst bed layers is calculated as:

$$N_r = 5.41 \times 10^5 \left(\frac{0.045}{205}\right) = 119 \quad \text{25-30 mesh}$$

$$N_r = 5.41 \times 10^5 \left(\frac{0.045}{32}\right) = 762 \quad \text{1/8" x 1/8" pellets}$$

The pressure drop through the fine mesh catalyst is then calculated as:

$$\Delta P_1 = \frac{(1260)\,(205)^{1.2}\,(0.045)^{1.8}\,(0.2)}{(0.336)^{1.7}\,(225)}$$

$$\Delta P_1 = 15.8 \text{ psid}$$

The pressure drop through the 1/8" x 1/8" pellets is calculated as:

$$\Delta P_2 = \frac{(3900)\,(32)\,(0.045)^2\,(1.87)}{(0.336)^{1.7}\,(210)}$$

$$\Delta P_2 = 14.7 \text{ psid}$$

The total pressure drop across the catalyst bed is then estimated as 30.5 psid. This is within the recommended design limits and no further iteration is required. Thus, the engine design is as follows:

Vacuum Thrust	=	100 lbf
Chamber Pressure	=	200 psia
Catalyst Bed Diameter	=	3.48 inches
Catalyst Bed Length	=	2.07 inches
Catalyst Bed Particle Size	=	0.2 inches, 25-30 mesh
		1.87 inches, 1/8" x 1/8" pellets
Catalyst Bed Pressure Drop	=	30.5 psid

The showerhead injector may be designed as follows. The number of orifices is calculated from:

$$N_o = 6\,A_B$$

$$N_o = 6\,(9.46) = 57 \text{ orifices}$$

The injector pressure drop is calculated from:

$$\Delta P_i = 0.15\, P_{cd\,\infty}$$

$$\Delta P_i = 0.15\,(200) = 30 \text{ psid}$$

The injector orifice diameter is calculated from:

$$D_o^4 = \frac{\dot{w}^2}{24\, \rho_g \left(\frac{\pi}{4}\right)^2 n^2 C_D^2\, \Delta P_i}$$

For the 100 lbf engine

$\dot{w}$ = 0.428 lbm/sec

ρ = 0.0364 lb/in^3

n = 57

C_D = 0.75

Therefore:

$$D_o^4 = 1.927 \times 10^{-7}$$

and

$$D_o = 0.021 \text{ inches}$$

The orifice spacing may be calculated from the equation

$$S = \frac{\pi n D_c}{N_T + \pi n^2 + \pi n}$$

For the 100 lbf engine:

D_c = 3.47 in.

N_T = 57

n = 4

Therefore:

$$S = \frac{\pi(4)(3.47)}{57 + \pi(16) + \pi(4)}$$

$$S = 0.364 \text{ inches.}$$

Therefore, the diameter of each orifice row is:

$$D_1 = 3.47 - 0.364(2) = 2.742 \text{ inches}$$

$$D_2 = 2.742 - 0.364(2) = 2.014 \text{ inches}$$

$$D_3 = 2.014 - 0.364(2) = 1.286 \text{ inches}$$

$$D_4 = 1.286 - 0.364(2) = 0.558 \text{ inches}$$

The number of orifices in each row is calculated to be:

$$n_1 = \frac{\pi(2.742)}{0.364} = 24$$

$$n_2 = \frac{\pi(2.014)}{0.364} = 17$$

$$n_3 = \frac{\pi(1.286)}{0.364} = 11$$

$$n_4 = \frac{\pi(0.558)}{0.364} = 5$$

The engine cold bed response time may be calculated from the two following equations:

$$t_1 = \frac{3.69 \times 10^4 V_c}{\dot{w}_\infty R T_{co}} \int_{0.01}^{0.8} \frac{d\eta}{\sqrt{\frac{(F-\eta)\eta}{(F-D)\eta + (D-1)Z}}\,\eta\sqrt{\frac{1}{Z}}}$$

$$t_2 = \frac{570 C_c (F-D)^{3/2}}{\dot{w}_\infty P_f} \int_{0.8}^{0.9} \frac{(2F - D\eta)\eta\, d\eta}{(F-D\eta)^{3/2}\left[F - D\eta - (F-D)\eta^2\right]}$$

where t_1 is the time for chamber pressure to rise to 80% of its steady state value and t_2 is the time for chamber pressure to rise from 80% to 90% of its steady state value. For the 100 lbf engine the following values apply:

$$F = \frac{P_f}{P_{cd\,\infty}} = \frac{300}{200} = 1.500$$

$$D = \frac{P_{cu\,\infty}}{P_{cd\,\infty}} = \frac{230.5}{200} = 1.153$$

$V_c = 10\ in^3$

$T_{co} = 520°R$

$C_c = 0.172\ Btu/°F$

$R = 18{,}528\ in\ lbf/lb\ mole\ °R$

$\dot{w}_\infty = 0.428\ lbm/sec$

$$\int_{0.01}^{0.8} \frac{d\eta}{\sqrt{\frac{(F-\eta)\eta}{(F-D)\eta + (D-1)Z}} - \eta\sqrt{\frac{1}{Z}}} = 1.265 \text{ (See Figure 25)}$$

$$\int_{0.8}^{0.9} \frac{(2F - D\eta)\eta\ d\eta}{(F-D\eta)^{3/2}\left[F - D\eta - (F-D)\eta^2\right]} = 0.375 \text{ (See Figure 27)}$$

Therefore:

$$t_1 = \frac{(3.69 \times 10^4)(10)(1.265)}{(0.428)(18{,}528)(520)} = 0.113 \text{ sec}$$

and

$$t_2 = \frac{(570)(0.172)(0.375)}{(0.428)(300)} = 0.286 \text{ sec}$$

Therefore, the predicted rise time to 80% of steady state chamber pressure is 113 milliseconds and the time to 90% of steady state chamber pressure is 399 milliseconds.

Ammonia dissociation for the 100 lbf engine design may be calculated from the following equation:

$$\ln\left(\frac{0.5}{1-X}\right) = 152.3\,\frac{G^{0.71}\,t}{d_p^{\,0.32}\,P}$$

For the engine design:

$$t = \frac{\epsilon L \bar{M} P}{G R T} = \frac{(0.336)(2.07)(200)(1000)}{(0.045)(113)(2260)(12)}$$

$t = 1.009$ ms

$G = 0.045$ lbm/in^2-sec

$P = 200$ psia

$d_p = 0.0119$ ft.

Therefore:

$$\ln\left(\frac{0.5}{1-X}\right) = \frac{(152.3)(0.045)^{0.71}\,(1.009)}{(0.0119)^{0.32}\,(200)}$$

$$\ln\left(\frac{0.5}{1-X}\right) = 0.3509$$

$$X = 64.8\%$$

Reverse Side Blank

PRECEDING PAGE BLANK NOT FILMED.

APPENDIX II

The following paragraphs illustrate the use of the design equations for a typical gas generator. The following gas generator requirements are assumed:

Chamber Pressure	=	300 psia
Propellant Flow Rate	=	0.25 lbm/sec
Ammonia Dissociation	=	75%

A bed loading of 0.045 lb/in^2-sec is chosen as a starting point for the design iteration. Using this bed loading, the chamber diameter is calculated as:

$$D_b = \sqrt{\frac{4}{\pi}\left(\frac{0.25}{0.045}\right)} = 2.66 \text{ inches}$$

For this bed diameter, an 0.2 inch layer of 25-30 mesh catalyst is used at the top of the catalyst bed with the remainder of the bed 1/8" x 1/8" cylindrical pellets.

Using the curves in Section 2.0, the catalyst bed porosity and specific surface area are estimated as:

$A_s = 204.5$	25-30 mesh granules
$A_s = 31.8$	1/8" x 1/8" pellets
$\epsilon = 0.34$	25-30 mesh granules
$\epsilon = 0.338$	1/8" x 1/8" pellets

The required bed length is then calculated from:

$$\ln\left(\frac{1-0.5}{1-X}\right) = 152.5\ \frac{G^{0.71}\ t}{d_p^{0.32}\ P}$$

$$t = \frac{\epsilon L \bar{M} P}{G R T}$$

$$t = \frac{(0.34)\ (L)\ (300)\ (1000)}{(0.045)\ (113)\ (2260)\ (12)}$$

$$t = 0.74\ L$$

$$\ln\left(\frac{1-0.5}{1-0.75}\right) = \frac{(152.5)\ (0.04)^{0.71}\ (0.831)\ L}{(0.0119)^{0.32}\ (300)}$$

$$L = \frac{(0.693)\,(300)\,(0.242)}{(152.5)\,(0.74)\,(0.111)}$$

$$L = 4.00 \text{ inches}$$

The Reynolds Number for flow through each layer of the bed is calculated as:

$$N_r = (5.41 \times 10^5)\left(\frac{0.045}{204.5}\right) = 119 \qquad \text{25-30 mesh}$$

$$N_r = (5.41 \times 10^5)\left(\frac{0.045}{32}\right) = 762 \qquad \text{1/8" x 1/8" pellets}$$

The pressure drop through the 25-30 mesh catalyst can be calculated as:

$$\Delta P_1 = \frac{(1260)\,(204.5)^{1.2}\,(0.045)^{1.8}\,(0.2)}{(0.34)^{1.7}\,(320)}$$

$$\Delta P_1 = 9.5 \text{ psid}$$

The pressure drop through the 1/8" x 1/8" cylindrical pellets is calculated as:

$$\Delta P_2 = \frac{(3900)\,(32)\,(0.045)^2\,(3.80)}{(310)\,(.16)}$$

$$\Delta P_2 = 19.2 \text{ psid}$$

The total catalyst bed pressure drop is nearly 30 psid which is within the recommended design limits and no further iteration is required. The gas generator design is then as follows

Propellant Flow Rate	=	0.25 lbm/sec
Chamber Pressure	=	300 psia
Ammonia Dissociation	=	75%
Catalyst Bed Diameter	=	2.66 inches
Catalyst Bed Length	=	4.00 inches
Catalyst Particle Size	=	0.2 inches, 25-30 mesh 3.8 inches, 1/8" x 1/8" pellets
Catalyst Bed Pressure Drop	=	29 psid

Reverse Side Blank

PRECEDING PAGE BLANK NOT FILMED.

NOMENCLATURE

a	=	An experimental constant
A_b	=	Cross-sectional area of catalyst bed, in^2
A_s	=	Catalyst specific surface area, in^2/in^3
b	=	An experimental constant
c	=	An experimental constant
C_c	=	Catalyst heat capacity, Btu/°F
C_{pg}	=	Gas heat capacity, Btu/lb °F
D	=	Ratio of chamber pressure upstream of catalyst bed to chamber pressure downstream of catalyst bed
D_b	=	Catalyst bed diameter, in
D_d	=	Ammonia diffusivity, in^2/sec
d_p	=	Average catalyst particle diameter determined from standard U. S. sieves, in.
d_s	=	Diameter of a spherical particle which has the same volume as the volume of the particle in question, in.
f	=	Frictional factor
F	=	Ratio of injection pressure to chamber pressure downstream of catalyst bed
G	=	Superficial mass velocity, lbm/in^2-sec
g_c	=	Gravitational constant, 32.17 ft/sec^2
ΔH_{rf}	=	Heat of reaction of hydrazine, Btu/lbm
I_s	=	Specific impulse, lbf-sec/lbm
K	=	An experimental constant
K_D	=	An experimental constant
k_g	=	Mass transfer coefficient, $lb/mole\text{-}psi\text{-}sec\text{-}in^3$
K_v	=	Volumetric particle shape factor

NOMENCLATURE (Cont'd)

L	=	Catalyst bed length, in.
$\bar{M}$	=	Average molecular weight of gas products, lb/lb mole
m	=	An experimental constant
N_r	=	Reynold Number
P_{cd}	=	Chamber pressure downstream of catalyst bed, psia
P_{cu}	=	Chamber pressure upstream of catalyst bed, psia
P_f	=	Propellant injection pressure, psia
q	=	An experimental constant
R	=	Universal gas constant, in-lbf/lb mole °R
T	=	Gas temperature, °R
t	=	Time, sec
V_c	=	Void volume in reactor, in^3
W_c	=	Weight of catalyst bed, lbm
$\dot{w}$	=	Propellant flow rate, lbm/sec
X	=	Fractional ammonia dissociation
Y_{NH_3}	=	Mole fraction ammonia

GREEK LETTERS

α	=	An experimental constant = 150
β	=	An experimental constant = 1.75
ϵ	=	Fractional void volume in catalyst bed
η	=	Fractional approach of downstream chamber pressure to steady state value
θ	=	Fractional approach of chamber temperature to steady state value
μ	=	Gas viscosity, lbm/in-sec

ρ_b = Ratio of catalyst weight to empty chamber volume, gm/cc

ρ_p = Ratio of catalyst particle weight to particle volume, gm/cc

ϕ_s = Catalyst particle sphericity

Reverse Side Blank

PRECEDING PAGE BLANK NOT FILMED.

REFERENCES

1. Rao, G.V.R., "Evaluation of Conical Nozzle Thrust Coefficient", ARS Journal, pages 606-607, 1959.
2. Ostle, Bernard, "Statistics in Research", Ames, Iowa, The Iowa State College Press, 1956.
3. Grant, A.F., Jr., "Basic Factors Involved in the Design and Operation of Catalytic Monopropellant-Hydrazine Reaction Chambers, Report No. 20-72" Pasadena: Jet Propulsion Laboratory, December 31, 1954 (Confidential).
4. Rocket Research Corporation, Contract AF 04(695)-550. May 1965, through March 1966.
5. Wrobel, J. R., "Effects of Fuel Inlet Temperature upon the Performance of a Monopropellant Hydrazine Reaction Chamber", Technical Memorandum No. 33-132. Pasadena: Jet Propulsion Laboratory, July 7, 1963.
6. Lee, D. H., "Performance Calculations of Monopropellant Hydrazine and Monopropellant Hydrazine-Hydrazine Nitrate Mixture", Technical Report No. 32-348, Jet Propulsion Laboratory, Pasadena, December 3, 1962.
7. Perry, John H., "Chemical Engineers Handbook", 4th Edition. New York: McGraw-Hill Book Company, Inc.
8. Brown, G.G., et al, "Unit Operations", New York, John Wiley and Sons, Inc., 1950.
9. Satterfield, Charles N.; Resnick, Hyman; and Wentworth, Ralph C., "Simultaneous Heat and Mass Transfer in a Diffusion Controlled Chemical Reaction".
10. Voge, H. H., et al, "Development of Catalysts for Monopropellant Decomposition of Hydrazine". Final Report, Contract NAS 7-97. Shell Development Company Report No. S-13889, October 1962 - June 1963.
11. McAdams, W. H., "Heat Transmission", New York: McGraw Hill Book Company, Inc., 1954.
12. Hougen, O. A. and Watson, R. M., "Chemical Process Principles", Volume III, New York. John Wiley and Sons, Inc.
13. Ergun, S., "Chemical Engineering Progress", 48, 89-94 (1952).